scientific reports

Check for updates

OPEN

Frequency stability improvement in EV-integrated power systems using optimized fuzzy-sliding mode control and real-time validation

Benazeer Begum[1], Narendra Kumar Jena[1], Binod Kumar Sahu[1]✉, Mohit Bajaj[2,3,4]✉, Vojtech Blazek[5] & Lukas Prokop[5]

The rapid growth in power demand, integration of renewable energy sources (RES), and intermittent uncertainties have significantly challenged the stability and reliability of interconnected power systems. The integration of electric vehicles (EVs), with their bidirectional power flow, further exacerbates the frequency fluctuation in the power system. So, to mitigate the frequency & power deviations as well as to stabilize the power system integrated with distributed generators (DGs) and EVs, robust & intelligent control strategies are indispensable. This study dedicates a novel Fuzzy-Sliding Mode Controller (FSMC) utilized for load frequency control (LFC). First, the dynamic response has been evaluated by using a Sliding Mode Controller (SMC), showcasing its robustness against external disturbances and parameter uncertainties. Second, to enhance the performance, fuzzy logic is integrated with SMC, leveraging its adaptability to create the FSMC controller. This FSMC has achieved the superiority by handling non-linearities, communication delays and parameter variations in the system. A significant contribution like the design and tuning of the controllers using a Modified Gannet Optimization Algorithm (MGOA) has been established. The potential of MGOA over GOA has been corroborated by convergence speed and precision through benchmark functions. Furthermore, the paper extensively analyzes the impact of EV integration to the frequency and tie-line power dynamics under varying regulation capacities and uncertain operating conditions. Comparative studies demonstrate that the MGOA-tuned FSMC achieves faster settling times, reduced overshoot, and improved stability metrics compared to conventional and state-of-the-art methods. Finally, the MATLAB-based simulation results are validated through real-time implementation on the OPAL-RT 4510 platform, confirming the robustness and practicality of the proposed methodology in addressing modern power system challenges involving high renewable penetration and EV integration.

Keywords Frequency stability, Load frequency control, Fuzzy-sliding mode controller, Sliding mode controller, Gannet Optimization Algorithm, Modified Gannet Optimization, Electric vehicles integration, Real-time simulation

At present, hybrid generating units are quintessential to integrate in an interconnected power system due to incessant power demand. In this context, hard efforts have been zeroed in to integrate the renewable sources (RSs) with the existing conventional power system. So, the intricacy of the system is magnified in the view of operation, reliability and stability of the system. The aberrant fluctuation of power demand and the intermittent characteristics of renewable sources create a gap between generation and demand[1,2]. But to yield a stable, secured and smooth operation of a power system, balance between generation and demand must be maintained. This insurmountable issue can't be solved by without a supplementary control as highlighted in[3,4] and the power balance technique is called as load frequency control (LFC). It controls the frequency deviation, power flow

[1]Department of Electrical Engineering, ITER, Siksha 'O' Anusandhan Deemed to Be University, Bhubaneswar, Odisha, India. [2]Department of Electrical Engineering, Graphic Era (Deemed to be University), Dehradun 248002, India. [3]Hourani Center for Applied Scientific Research, Al-Ahliyya Amman University, Amman, Jordan. [4]College of Engineering, University of Business and Technology, 21448 Jeddah, Saudi Arabia. [5]ENET Centre, CEET, VSB-Technical University of Ostrava, 708 00 Ostrava, Czech Republic. ✉email: binoditer@gmail.com; mohitbajaj.ee@geu.ac.in

in the tie-line with effectual load sharing. Inadequate control causes oscillations in the system frequency and incessant fluctuation culminates to blackouts.

Now-a-days, attraction of electric vehicle (EV) is increasing rapidly to substitute the fossil fuel based vehicle, in turn the environment can be freed from chemical laden gases[5]. In this perspective, the vehicle to grid technology is advancing swiftly and the growth of plug-in hybrid EVs may surpass hundred million a year by 2050 as inculcated by Falahati et al.[6]. In EV aggregators the battery charges or discharges with a high rate. So, the change in power output of EV aggregator is faster than the other generating sources, in turn causes a huge power imbalance in the power network. To maintain the power balance in the system, LFC is quintessential which has been discussed eloquently in[7–9]. Also, the EV aggregators introduce time varying delays in the LFC system. This time delay deteriorates the system performance and even causes instability in the system[10]. So, integration of EVs, RSs and distributed generators (DGs) to the existing power system is more vulnerable to the frequency deviation in the system.

For the above problem, an effective LFC control strategy is imperative to balance the power generation and demand swiftly. So, various control strategies like conventional control[11–17] non-integer based conventional control[15,18–23], optimal control[24–26], intelligent control[27–30], non-linear & robust control[31–39] and many more have been addressed to mitigate the LFC issues. Pappachen et al.[11] proposed a proportional- integral (PI) controller to eradicate the frequency deviation in a three-area power system under different power transaction condition & under superconducting magnetic energy storage device. Nanda et al.[13] has carried a work to regulate the frequency using only I controller dwelled with governor speed regulation parameter & frequency bias parameter. But, in this case the response has performed sluggish response showing a very magnified undershoot and overshoot. A new kind of work like integration of distributed generators (DGs) to a conventional power system has been presented by Das et al.[14]. In this work, the authors have discussed elaborately the issues of DGs in a system and the LFC problem has been tackled by using a PI controller. To have a prompt control action, a 2-stage controller has been modeled as highlighted in[12,15] to mitigate the frequency and power fluctuation in the power network. Further, the fractional order (FO) classical controllers have produced better proven ameliorated performance in the LFC strategy. A cascade controller aided with FO[15,23] has been endorsed in a multi-area system to regulate the frequency and also the improved performance over its cascade controller has been corroborated adequately. Arya[9] has employed the FO-ID controller to a system to reap better frequency stability in the presence of EV. Further, Arya[22] has performed the LFC issue using tilted-ID controller in an interconnected power system. Similar kinds of work have been carried out like Sahu et al.[18], Gorripotu et al.[19], Ahmed et al.[20], Guha et al.[21]. In these works, the authors have presented the extra features of FO controller aided with classical controllers. But the settling times is sacrificed to yield better response. And, the system response with renewable sources has not produced an astounding response.

Jabari et al.[40] proposed an innovative artificial intelligence-based multistage controller that enhances load frequency control (LFC) by dynamically adapting to system uncertainties. The controller demonstrated significant improvements in frequency regulation through its ability to address multi-stage dynamics and optimize performance in real-time. Dev et al.[41] introduced the Walrus optimization algorithm to improve both LFC and automatic voltage regulation in interconnected power systems. The study highlighted the algorithm's superior performance in achieving faster convergence and enhanced stability metrics. Daraz et al.[42] examined frequency stabilization in interconnected systems with high penetration of renewable energy sources and energy storage systems. Their work demonstrated the efficacy of coordinated control strategies in mitigating frequency deviations and managing power imbalances caused by renewable intermittency. Mahmoud et al.[43] employed whale optimization algorithm-based fractional-order proportional-integral (FOPI) controllers to mitigate harmonics and voltage instability in modern distribution grids. The study emphasized the controller's robustness in maintaining system stability under varying operating conditions. Ardjoun et al.[44] proposed a robust control strategy to enhance the frequency support capability of grid-tied photovoltaic systems, addressing the challenges posed by the variable nature of solar energy. The study demonstrated significant improvements in system stability through advanced control techniques. Davoudkhani et al.[45] presented the maiden application of the mountaineering team-based optimization algorithm for optimizing a 1PD-PI controller in islanded microgrids. Their work highlighted the controller's efficacy in managing renewable energy sources and achieving robust frequency regulation. Ekinci et al.[46] introduced a hybrid educational competition optimizer combined with pattern search techniques to regulate the frequency of a photovoltaic and reheat thermal power system. The study demonstrated enhanced controller performance through a cascaded PDN-PI configuration. Gopi et al.[47] proposed a novel rat swarm optimization algorithm for tuning LFC controllers, emphasizing the algorithm's efficiency in improving the stability and dynamic response of power systems. Davoudkhani et al.[48] developed a robust LFC strategy using a 1PD-3DOF-PID controller integrated with mobile EV energy storage for islanded urban microgrids. The study highlighted the controller's ability to handle disturbances and improve frequency regulation in complex microgrid scenarios. Daraz et al.[49] investigated the stabilization of load frequency in hybrid power systems with renewable energy integration, EVs, and capacitive energy storage. The research demonstrated effective stabilization of frequency deviations and power fluctuations through advanced control mechanisms. Begum et al.[50] applied an intelligent fuzzy logic-based sliding mode controller to address frequency stability issues in deregulated power systems, validating their results through OPAL-RT simulations. Their study demonstrated the controller's ability to handle uncertainties and improve dynamic performance. Daraz et al.[51] explored frequency regulation strategies for interconnected hybrid power systems with EV integration, emphasizing the importance of robust control mechanisms to mitigate system disturbances. Kalyan et al.[52] investigated the frequency regulation of geothermal power plant-integrated systems using a 3DOFPID controller. Their work demonstrated the controller's capability to manage complex dynamics and achieve enhanced frequency stability. Additionally, Kalyan et al.[53] employed the water cycle algorithm to optimize a Type II fuzzy

controller for LFC in multi-area systems with communication time delays, achieving superior stability metrics and addressing delay-induced challenges effectively.

Similarly, there have been studies those collectively emphasize advanced control strategies and optimization techniques in addressing stability, performance, and dynamic challenges in energy and control systems. They highlight the interconnection between robust control mechanisms, optimization methods, and the need for adaptive solutions in systems with renewable energy sources and hybrid configurations. Dunna et al.[54] explore a super-twisting MPPT control integrated with a higher-order sliding mode observer (HOSMO) for grid-connected PV and battery systems. The focus is on enhancing the efficiency and stability of maximum power point tracking (MPPT) under dynamic and fluctuating conditions, highlighting the critical role of advanced control mechanisms in renewable energy systems. Izci et al.[55] address the stability of automatic voltage regulation (AVR) systems using a fractional-order PID controller combined with a double-derivative controller, optimized via the Mountain Gazelle Optimizer (MGO). This study emphasizes the importance of robust control strategies and optimization for ensuring stability in systems experiencing dynamic changes. Aribowo et al.[56] and[57] focus on optimizing PID controllers for DC motors using the Mountain Gazelle Optimizer. These works highlight the effectiveness of advanced optimization algorithms in tuning control parameters, ensuring system performance and stability. The use of such optimization techniques is particularly relevant for managing systems with dynamic operational characteristics. Premkumar et al.[58] propose an intelligent multi-objective optimization approach for hybrid power systems, incorporating stochastic renewable sources and FACTS devices. The study demonstrates the significance of multi-objective optimization in balancing reliability, stability, and performance in hybrid systems, particularly in environments with uncertain and variable inputs. Pandya et al.[59] extend this concept by analyzing hybrid power systems through a multi-objective RIME algorithm, addressing security constraints and uncertainty in load dispatch and power flow. This work integrates techno-economic considerations with optimization, illustrating the critical role of adaptive strategies in managing hybrid systems. Alsmadi et al.[60] utilize fuzzy logic for digital system model order reduction while preserving system behavior, providing insights into simplifying and optimizing control systems without compromising performance. This methodology is applicable for maintaining operational efficiency in complex interconnected systems. Abualigah et al.[61] present a filtered PID controller for aircraft pitch control, tuned using the Sinh-Cosh optimizer. While centered on aviation, the principles of optimization and fine-tuned controller design can be applied broadly to other dynamic systems requiring precise control. Alrashed et al.[62] introduce a control strategy for a DVR compensator using an optimized PD controller with an adaptive notch filter. This method improves system stability during disturbances, demonstrating the adaptability of control strategies in managing dynamic load and fault conditions in power systems. Fadheel et al.[63] propose a hybrid Sparrow Search Optimized Fractional Virtual Inertia Control strategy for frequency regulation in multi-microgrid systems. This work addresses the challenges of decentralized control and frequency stability in microgrids with renewable energy integration. Abualigah et al.[64] integrate an artificial rabbits optimizer with a PID-F controller for dynamic systems. This approach highlights the utility of novel optimization techniques for enhancing controller performance in environments with fluctuating operational demands. Izci et al.[65] refine AVR system control using the Sinh-Cosh optimizer, focusing on enhancing stability through precise controller parameter tuning. The study demonstrates the value of innovative optimization approaches in achieving robust control in dynamic systems. Izci et al.[66] propose a novel AVR control scheme using a modified artificial rabbits optimizer, emphasizing the flexibility of optimization methods in improving control performance across varying system conditions. Altawil et al.[67] apply the Slap Swarm Algorithm to optimize fractional-order PI controllers for voltage regulation in grid-connected PV systems. Their work highlights the importance of advanced optimization techniques in managing the challenges posed by renewable energy systems, such as variability and integration complexities. Abualigah et al.[68] use the Elite Opposition-Based Artificial Hummingbird Algorithm for designing fractional-order PID controllers, demonstrating the role of innovative optimization techniques in improving system performance and dynamic response. Sarayrah et al.[69] study damping control strategies for inter-area power systems, emphasizing predictive control to mitigate oscillations. This work underscores the necessity of effective damping strategies in maintaining stability in interconnected power systems.

Some researchers have paid their interest in optimal control to execute frequency response in different types of power systems. Elaydi and Mohammed[24] have designed a linear quadratic regulator (LQR) to address the LFC issue in a power system. Ali et al.[25] proposed a sister controller called a linear quadratic Gaussian (LQG) and used this controller to performed the transient response of a system with respect to the power imbalance in the system. Alhelou et al.[26] proposed a state observer with dynamic state estimation to evaluate the performance of a power system under various generation and demand characteristics. Although, these controllers show inherent robustness but it is too difficult to measure all these states during its system dynamic. Also, the performance of these controllers under all sorts `of intermittent uncertainties have not discussed profusely.

For a prompt and effective control action in LFC, some researchers have laid a great emphasis on intelligent control strategy. In this context, Biswas et al.[27] have included the Dish-Stirling Solar-thermal system in every area to study the LFC problem. To find the frequency response, PID controller assisted by fuzzy logic has been employed. Also, the paper has addressed the load sharing pattern to find the control areas. Sahoo et al.[28] have formulated a self-adapted fuzzy controller to stabilize the frequency under different critical operating conditions. The proficiency of the fuzzy controller has been augmented by a two branched type-2 configuration. In this perspective, Kumari et al.[29] have performed and compared the response produced by type-2 fuzzy controller in comparison to conventional fuzzy controller. In this work, the LFC of the system has been determined by integrating renewable sources. Another piece of work has been corroborated by composing the predictive control theory with fuzzy logic as explored by Wang et al.[30]. In this work, the LFC has been discussed in the presence of wind energy conversion system. In these works, it has been observed that the intelligent control has

stabilized the power system under power imbalance condition. Still, the application of fuzzy controller combined with other control topology has a great scope in this field which is yet to be explored.

In practical, the integration of DGs including renewable sources, EVs and micro-grids causes the instability in the power system. So, these uncertainties including low/no inertia generating units puts the system in trouble by which the frequency deviation becomes a critical issue. In this regard, some researchers have focused in robust control technology. Tianand Chen[31] proposed H_∞ controller to stabilize the system frequency effortlessly in a power system. In this work, the robustness of the controller has been articulated under different deception threat. A similar kind of work carried by Xiahou et al.[32] and in this work, a perturbation observer has been designed corresponding to the perturbation caused by the power imbalance caused in the system. The designed controller has performed significantly to control the system frequency deviation. Also, the controller has performed remarkably to the time-delay threat that happens in a system. Shen et al.[33] has presented an H_∞ robust controller to find the transient behavior against external disturbance in a power system. Here, the designed controller has performed better in comparison to other techniques and the controller has supported extensively to the wide range of delay. Apart from these controllers, non-linear controller named sliding mode controller (SMC) has been bestowed in different power systems integrated with/without renewable sources, DGs, EVs or micro-grids for LFC study. The severe uncertainties and the discrepancies (external perturbation/parameter variation of plant or controllers/parasitic dynamics) occurs between the dynamics of real system and the model designed with controllers force the control engineers to design a non-linear and robust controller as discussed in[34,35]. Wang et al.[36] have designed a SMC controller to study the LFC in a multi-area system injecting wind energy system and EV. An SMC controller having third order sliding surface designed by Shouran et al.[37] has been applied to a 2-area system to evaluate the frequency response. In this work, the superior performance of SMC over FLC has been highlighted. The potential of SMC controller in the conglomeration with FL has been illustrated in[38]. The capability of this controller for the stability of the system has been advocated under time delay and external perturbation condition. Ansari et al.[39] proposed an event triggered SMC controller to execute the transient response under various uncertainties and disturbances in a system. In LFC, to reduce the disturbance effect, the designed observer controls the control signal in feed forward way. So, the SMC controller becomes more robust.

With a suitable control structure, paramount design of controller is necessary to have robust performance. For this, optimization technique is indispensable. In the perspective of LFC work, various researchers have applied different algorithms extensively such as genetic algorithm[11,14,25], selfish herd optimization[12], bacterial foraging[13], whale optimization[18], differential evolution[19], imperialist competitive algorithm[20], particle swarm optimization[70] etc. Despite having their own edge to particular problem may not produce satisfactory result for other kinds of problems. So, the newly evolved algorithms may be endorsed to optimize the problems effectively.

Contemplating the literature review as discussed above, the key findings have been amassed as:

i. Integration of renewable energy sources causes power fluctuation which creates a challenge for frequency security. To mitigate this frequency and tie-line power oscillations, an effective and robust controller is obligatory.
ii. Penetration of EVs into an interconnected power system makes the system more intricacy. So, to handle this impact, an intelligent controller is quintessential to address the LFC issue in a system.
iii. Again, to regulate the frequency deviation due to communication delay and parameter variation in EV system, a robust controller is necessary.
iv. SMC controller is the best approach to reap stable and robust dynamic response in a system incurring intermittent and external disturbances, parametric variation in the system and communication delay.
v. Again, fuzzy assisted SMC (FSMC) controller may enrich the performance immensely which has not addressed adequately. So, it has a greater scope to investigate and employ in an interconnected system for the LFC problem.

The above findings suggest that the effective LFC technique can be executed by a robust controller designed by an optimization technique. Here, the proposed model has been established by an intelligent FSMC controller and its parameters have been enumerated by using Gannet Optimization Algorithm (GOA) and modified-GOA (MGOA) algorithms.

The prime objectives accompanying the major contribution in this work have been articulated as follows:

i. An interconnected power system carrying conventional, RESs and EVs has been modeled to regulate the fluctuation of frequency and power flow in the tie-line.
ii. An SMC controller has been designed endorsing GOA algorithm to deploy in LFC technique for the proposed model.
iii. Further, to improve the dynamic response of the system, an intelligent GOA-FSMC controller has been utilized.
iv. To enhance the potential of the GOA algorithm, it has been modified and the modified algorithm has been applied to design the SMC and FSMC controller to bestow a robust performance in the system.
v. To corroborate the potential of the modified GOA, some benchmark functions' performance and convergence curve of GOA and MGOA has been examined.
vi. The efficacy of MGOA over well-established particle swarm optimization (PSO) has been presented.
vii. Robustness of the controller has been presented by varying EV parameters and system parameters.
viii. Finally, the dynamic response of the test model under MATLAB environment has been validated through OPAL-RT-4510.

System modeling

A power system model of three-area has been taken to study and enhance the response as shown in Fig. 1. The model includes thermal, hydro, gas, distributed generators and EVs. In area-1, thermal unit has been integrated with DGs and EVs. In DG system, renewable sources like solar and wind energy conversion systems have been integrated. Besides this, geo-thermal power plant (GTPP) in addition to conventional diesel engine generator (DEG) has been integrated in it. In area-2, two conventional sources like hydro and thermal power stations have been integrated. Another variant of power source like gas energy conversion system has been integrated with the thermal power plant. In addition to this, EVs have been integrated in area-2 and area-3, also. The necessary non-linearities like generation rate constraint (GRC), governor dead band (GDB), boiler dynamics (BD) and up/down regulation in respective generating units have been considered. With an extensive study, the model of each generating unit has been illustrated below. The proposed model in transfer function domain has been portrayed in Fig. 2.

Thermal power system

The linearized model of the thermal power generator in frequency domain has been presented in the Fig. 2. The model has been expressed in transfer function form which is consisting of reheat unit, GRC, GDB and BD. The GRC and BD transfer function blocks have been shown in Fig. 3. Here, a GRC of 3%/min has been taken. The model and the necessary parameters have been followed from[9,22,71] and it's modeling equations have been provided below. The transfer function of the turbine and the reheat turbine has been given in Eqs. (1) and (2).

$$G_{1TT}(s) = \frac{1}{1 + sT_{TH_1}} \tag{1}$$

$$G_{1RT}(s) = \frac{1 + K_{RT1}T_{RT1}s}{1 + sT_{RT1}} \tag{2}$$

where, T_{TH_1} is the time constant of thermal turbine, K_{RT1}& T_{RT1} are the gain and time constant of reheat-turbine.

Hydro-power system

The hydro-power generation system has governor, transient droop compensator and turbine units. The model & it's parameters have been taken from[71]. The data of these parameters have been provided in appendix (supplementary material file). The nonlinearity, GRC of 270%/min for rising & 360%/min for lowering operation

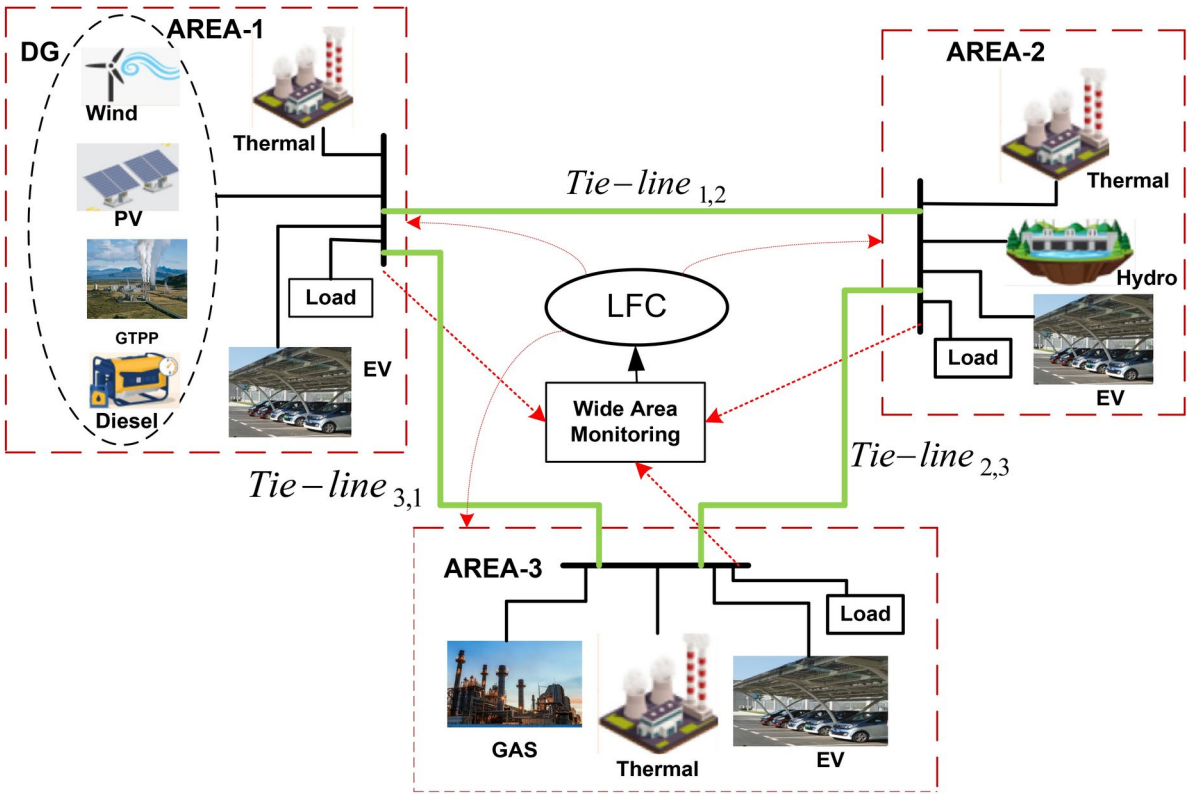

Fig. 1. Three-area interconnected power system.

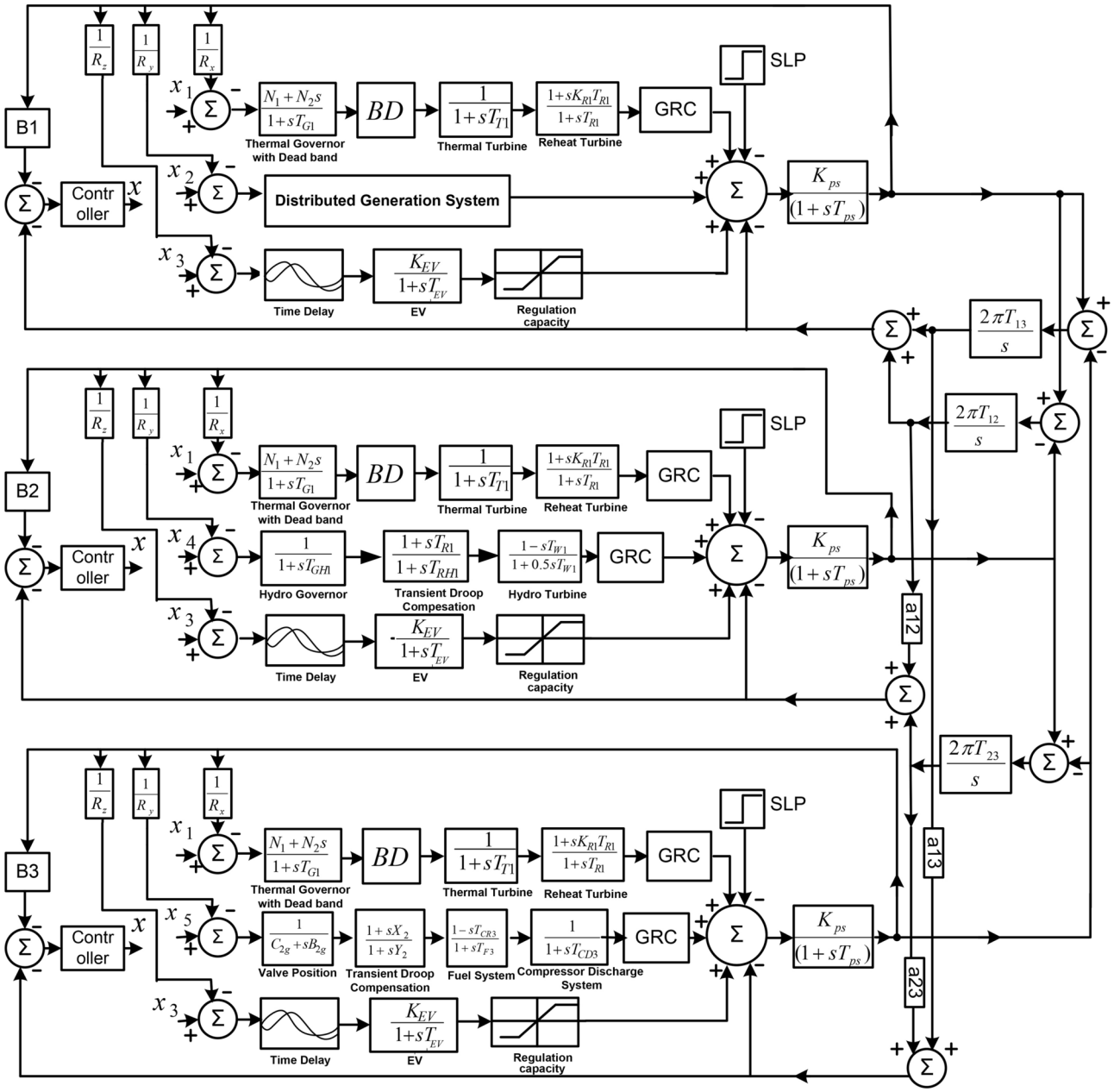

Fig. 2. Block diagram of proposed system.

has been adopted in this proposed model as discussed in the article[3,9]. The transfer function of governor, droop compensation and turbine is given in Eq. (3)-(5) respectively.

$$G_{1HG}(s) = \frac{1}{1 + sT_{HG1}} \tag{3}$$

$$G_{1TDC}(s) = \frac{1 + sT_{R1}}{1 + sT_{RH1}} \tag{4}$$

$$G_{1HT}(s) = \frac{1 - sT_{W1}}{1 + 0.5sT_{W1}} \tag{5}$$

where,T_{HG1} = time constant of governor,T_{R1} = speed governor rest time,T_{RH1} = droop constant of the governor, &T_{W1} = nominal start time of the turbine.

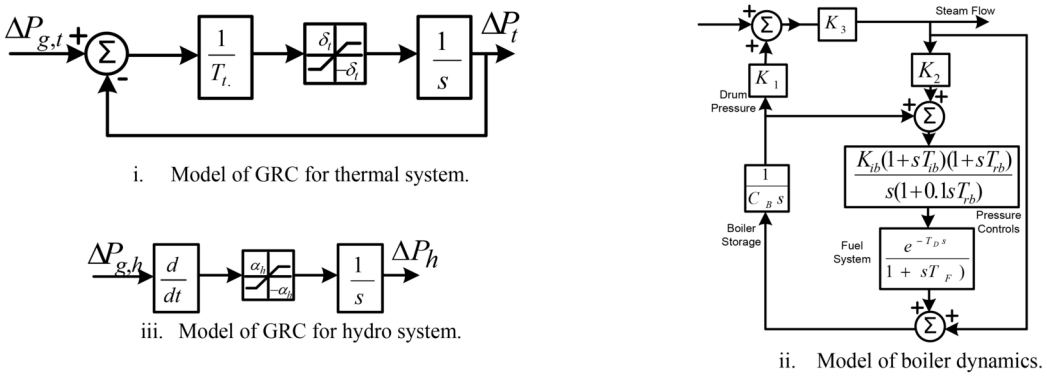

Fig. 3. Block diagram of GRC and BD.

Gas power system

The gas power unit consists of valve position block, transient droop compensation block, fuel system and compressor discharge system block. The dynamic equation of each block is given in Eqs. (6)–(9). The data of each block has been taken from[71] and depicted in the appendix. Here, the GRC of 2%/min has been taken as discussed in[12,71].

$$G_{1VP}(s) = \frac{1}{B_{2g} + C_{2g}} \tag{6}$$

$$G_{2TDC}(s) = \frac{1 + X_2 s}{1 + Y_2 s} \tag{7}$$

$$G_{1FS}(s) = \frac{1 - T_{CR3} s}{1 + T_{F3} s} \tag{8}$$

$$G_{1CDS}(s) = \frac{1}{1 + T_{CD3} s} \tag{9}$$

Geothermal power plant (GTPP)

In geothermal system, the thermal energy is extracted and utilized from the Earth's interior. The thermal energy is extracted through wells. The reservoirs are called as hydrothermal or enhanced geothermal according their process of extraction. The governor and turbine model of GTPP have been provided in Eqs. (10) & (11).

$$G_{G1}(s) = \frac{1}{T_{gtpp,g}\, s + 1} \tag{10}$$

$$G_{T1}(s) = \frac{1}{T_{gtpp,t}\, s + 1} \tag{11}$$

where, $T_{gtpp,g}$ = time constant of governor & $T_{gtpp,t}$ = time constant turbine which have been taken from[2,71] as provided in appendix.

Solar photovoltaic (SPV)

Generally, power extraction in PV depends on degree of irradiance and ambient temperature[72]. Based on this, the harvested power has been expressed in Eq. (12). The required expression and data have been followed from[2,22,71]. For the irradiance, a range 200W/m^2 to 1200W/m^2 has been considered.

$$P_{sp} = \eta_{sp}\, A_{\mathrm{mod}\ ule}\, \varphi_{irrd}\, (1 - 0.005\, (T_{at} + 25)) \tag{12}$$

Here,η_{sp} = efficiency of the solar cell, $A_{\mathrm{mod}\ ule}$ = irradiance-swept area, φ_{irrd} = irradiance, and T_{at} = ambient temperature. The transfer function model of SPV has been expressed as in Eq. (13).

$$G_{1SPV}(s) = \frac{K_{1SPV}}{1 + sT_{1SPV}} \tag{13}$$

where, K_{1SPV} and T_{1SPV} are the gain & time constant of SPV plant. The data of modeling parameter are taken from[71] and the same has been given in the appendix.

Diesel engine generator (DEG)

In DG unit, wind and solar system generates very fluctuating power due to their intermittent nature. To overcome this fluctuation, a diesel engine is employed in a DG unit with speed governor. The frequency domain dynamic model of DEG[2,14,15] has been provided in Eq. (14).

$$G_{1DEG}(s) = \frac{K_{1\,\mathrm{deg}}}{1 + sT_{1\,\mathrm{deg}}} \tag{14}$$

where, $K_{1\,\mathrm{deg}}$&$T_{1\,\mathrm{deg}}$ are the gain & time constant of DEG. The model and it's parameters have been taken from[71] and the data are given in the appendix.

Wind turbine system

In wind energy system, power fluctuates vehemently. So, in turn, the power fluctuates. Here, the total power captured by the swept area (A_{1R}) of the blade is not converted into electrical energy. The converted power to the total power is called the conversion ratio (C_{1P}) under a particular air density (ρ_{1air}). The extracted power equation has been provided in Eq. (15). For this power extraction, a wind speed (V_{1w}) range has been chosen i.e. ranging from cut-in (6 m/s) speed to cut-out speed (24 m/s).The necessary data and the power equation have been followed from[71]. And, the expression for the C_{1P} has been given in Eq. (16).

$$P_{1wts} = 0.5\rho_{1air}\, A_{1R}\, C_{1P}\, V_{1w}^3 \tag{15}$$

$$C_{1P} = (0.44 - 0.167\beta)\sin\left(\frac{\pi(\lambda - 3}{15 - 0.3\beta}\right) - 0.0184(\lambda - 3)\beta \tag{16}$$

where, λ and β are tip speed ratio & pitch angle respectively.

The frequency domain model for WTS[13,29,35] is given in Eq. (17).

$$G_{1WTS}(s) = \frac{K_{1wts}}{1 + sT_{1wts}} \tag{17}$$

where,K_{1wts},T_{1wts} are the gain and time constant of WTG. The data of the modeling parameters are taken from[71] and given in appendix.

Electric vehicle

The transfer function model of Electric Vehicle (EV)[6,9,36] is given in Fig. 2, including a dead band. Here, the control of EV with different regulation capacity has been considered. Further to make the model more realistic, a time delay[7,73] has been added. Due to the available regulation capacity the EV's parameters exhibit very strong uncertainty[74,75]. Generally, we have upper regulation capacity (URC) and down regulation capacity (DRC). URC is found by minimizing loading effect and DRC is found by increasing the loading effect in EV. Under this process, power is transferred in to-and-fro with the grid. The detailed variation and the values of DRC & URC have been given in Table *9. The model and it's data are taken from[76]. Equation (18) is the transfer function model which has been used in this work. Here, K_{EV} = gain for and T_{EV} = charging/discharging time constant.

$$G_{EV}(s) = \frac{K_{EV}}{1 + sT_{EV}} \tag{18}$$

Power system

From Fig. 2, the dynamic equation for the power system can be expressed as in Eq. (19).

$$\Delta \dot{f}_i = \frac{K_{ps}}{T_{ps}}\left(\Delta P_{s,i} - \Delta P_{L,i} - \Delta P_{tie,ij}\right) - \frac{\Delta f_i}{T_{ps}} \tag{19}$$

$$\begin{aligned}\Delta P_{s,1} &= \Delta P_{Thermal} + \Delta P_{DG} + \Delta P_{EV} \\ &= G_{Thermal}\left(u_{smc\,1} - \frac{\Delta f_1}{R}\right) + G_{DG}\left(u_{smc\,2} - \frac{\Delta f_1}{R}\right) + G_{EV}\left(u_{smc\,3} - \frac{\Delta f_1}{R}\right)\end{aligned} \tag{20}$$

$$\Delta P_{tie,12} = \frac{2\pi T_{12}}{s}\left(\Delta f_1 - \Delta f_2\right) + \frac{2\pi T_{13}}{s}\left(\Delta f_1 - \Delta f_3\right) \tag{21}$$

where, $i = 1,\ 2\ \&3$. $G_{Thermal}$, G_{DG} & G_{EV} are transfer function of thermal plant, DGs & EV respectively.

Methodology

A multi-area power system as in Fig. 2 has been taken for the LFC study. A DG unit including EV has been integrated. In EV, regulation capacity has been considered as carried by the researcher in[76]. To mitigate the frequency deviation, PID, SMC and Fuzzy-SMC controllers have been employed. These controllers have been designed by applying GOA technique. Further to enhance the performance, modified GOA has been applied to reap better response. The errors of this model during the optimization have been evaluated by ITAE objective function which has been provided by Eq. (22).

$$J_{objective\ fn} = \int_0^T \left[|\Delta f_1| \cdot t + |\Delta f_2| \cdot t + |\Delta f_3| \cdot t + |\Delta p_{tie12}| \cdot t + |\Delta p_{tie23}| \cdot t + |\Delta p_{tie31}| \cdot t\right] dt \quad (22)$$

Also, in the process of tuning various constraints have been considered as given below.

$$\begin{cases} 0 < k_p \leq 5 \\ 0 < k_i \leq 5 \\ 0 < k_d \leq 5 \end{cases} \quad for\ PID/FPID\ controllers$$

$$\begin{cases} -20 < x \leq 20 \\ -20 < y \leq 20 \\ -20 < z \leq 20 \end{cases} \quad for\ SMC/FSMC\ controllers$$

Finally, to validate the MATLAB result, OPAL-RT has been used by keeping the same tuned parameters of these controllers.

Control technique

Fuzzy-PID controller

Classical controller seldom shows robust performance against wide range of perturbation and uncertainties. Also, PID controller is very sensitive to non-linearities present in a complex higher order system. But, the PID controller becomes more intelligent in the conglomeration with fuzzy logic, although the design of membership function is a very cumbersome and difficult task. In this controller, the error ($e(t)$) and the derivative of error ($\dot{e}(t)$) are processed through the PID controller by which the actuating signal becomes more effective to minimize the error. The details of fuzzy logic can be referred from[27–29]. The expression for PID controller has been provided in Eq. (23). In this equation, $k_{p,i}$,$k_{i,i}$,$k_{d,i}$ are the proportional integral and derivative gains respectively. Here, i stands for no of controllers.

$$u_{PID,i}(t) = k_{p,i} * e(t) + k_{i,i} * \frac{de(t)}{dt} + k_{d,i} * \int e(t)dt \quad (23)$$

The FPID control structure has been portrayed in Fig. 4a. The triangular membership functions of a set five has been provided as in Fig. 4b. The fuzzy rules have been set as given in Table 1 which has been referred from[28]. In Table 1, $'Neg'_{lg}$,$'Neg'_{sm}$,$'Pos'_{lg}$,$'Pos'_{sm}$ & $'Z'$ stand for negative large, negative small, positive large, positive small& zero respectively.

Fuzzy-sliding mode controller

The non-linear control structure, named as SMC controller, was proposed by Russian engineers in the early 1950[77]. Subsequently, the SMC controller has gained a high momentum in the field of research around the globe due to it's substantial stable & robust performance against intermittent uncertainties. To design an SMC controller, three key steps to be endorsed as stated below.

a. Designing of sliding surface ($S(t,e)$): A suitable sliding surface is modeled by which convergence and stability are enabled.
b. Existence condition with switching logic: Existence condition is stressed by which it slides around the sliding manifold. And the switching logic dictates the controller to change it's designed gain according to the state's position change.
c. Designing of control law: A properly designed control law ensures the states of the proposed system to adhere the desired trajectory being on the sliding surface.

The sliding surface for SMC controller in this proposed non-linear system has been provided in Eq. (24) and it has been referred from[78,79].

$$S = \left(\frac{d}{dt} + \alpha_x\right)^n * e \quad (24)$$

Here, error in terms of area control error (ACE) can be represented as $e = \Delta ACE_{ref} - \Delta ACE_{meas}$ and from Fig. 2, $\Delta ACE = -(B * \Delta f_i + \Delta P_{tie,ij})$. α_x(designed constant) > 0,n=order of the sliding surface. For, $n = 1$, the sliding surface is given in Eq. (25).

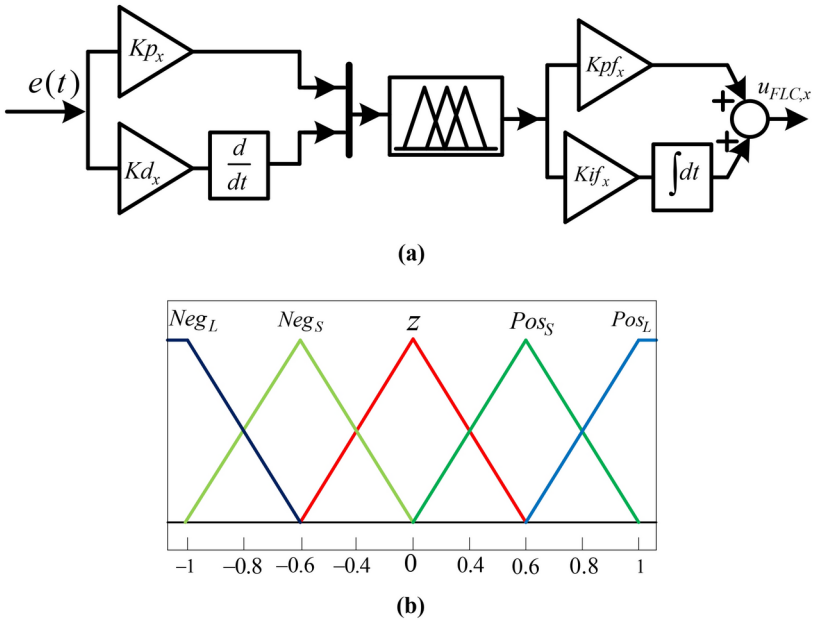

Fig. 4. (**a**) Fuzzy-PID Control structure. (**b**) Membership function structure of Fuzzy-PID controller.

$\dot{e}(t)$ / $e(t)$	Neg_{lg}	Neg_{sm}	Z	Pos_{sm}	Pos_{lg}
Neg_{lg}	Neg_{lg}	Neg_{lg}	Neg_{sm}	Neg_{sm}	Z
Neg_{sm}	Neg_{lg}	Neg_{sm}	Neg_{sm}	Z	Pos_{sm}
Z	Neg_{sm}	Neg_{sm}	Z	Pos_{sm}	Pos_{sm}
Pos_{sm}	Neg_{sm}	Z	Pos_{sm}	Pos_{sm}	Pos_{lg}
Pos_{lg}	Z	Pos_{sm}	Pos_{sm}	Pos_{lg}	Pos_{lg}

Table 1. Applied rule-base for Fuzzy-PID controller.

$$\begin{aligned} S &= \frac{de}{dt} + \alpha_x e \\ &= \frac{d(\Delta ACE_{ref} - \Delta ACE_{meas})}{dt} + \alpha_x(\Delta ACE_{ref} - \Delta ACE_{meas}) \\ &= -B_1\Delta \dot{f}_{i,ref} - \Delta \dot{P}_{tie\ ij,ref} + B_1\Delta \dot{f}_{i,meas} + \Delta \dot{P}_{tie\ ij,meas} \\ &\quad + \alpha_x\left(-B_1\Delta f_{i,ref} - \Delta P_{tie\ ij,ref} + B_1\Delta f_{i,meas} + \Delta P_{tie\ ij,meas}\right) \end{aligned} \tag{25}$$

For area-1, the sliding surface as in Eq. (25) can be simplified using Eqs. (19)-(21):

$$\begin{aligned} S &= B_1\Delta \dot{f}_{1,meas} + \Delta \dot{P}_{tie\ 12,meas} + \alpha_x\left(B_1\Delta f_{1,meas} + \Delta P_{tie\ 12,meas}\right) \\ &= \frac{B_1K_{ps}}{T_{ps}}\left(\Delta P_{s,1} - \Delta P_{L,1} - \Delta P_{tie,12}\right) - \frac{\Delta f_1}{T_{ps}} + 2\pi T_{12}\left(\Delta f_1 - \Delta f_2\right) + 2\pi T_{13}\left(\Delta f_1 - \Delta f_3\right) \\ &\quad + \alpha_x\left(B_1\Delta f_{1,meas} + \Delta P_{tie\ 12,meas}\right) \end{aligned} \tag{26}$$

For the existence condition, a Lyapunov function has been endorsed from[38,78,79] as provided in Eq. (27).

$$V = \frac{S^2}{2} \tag{27}$$

To be stable, the first differentiation of the energy function should be negative which has been provided in Eq. (28).

$$\begin{aligned} & V^{\cdot} < 0 \\ & \Rightarrow S.S^{\cdot} < 0 \end{aligned} \tag{28}$$

Proof: Here, the sliding surface function, S has been taken as derived in Eq. (26)

$$\begin{aligned} V^{\cdot} &= S * S^{\cdot} \\ &= S * \frac{d}{dt}\left[\begin{array}{l} \frac{B_1 K_{ps}}{T_{ps}}\left(\Delta P_{s,1} - \Delta P_{L,1} - \Delta P_{tie,12}\right) - \frac{\Delta f_1}{T_{ps}} + 2\pi T_{12}\left(\Delta f_1 - \Delta f_2\right) + 2\pi T_{13}\left(\Delta f_1 - \Delta f_3\right) \\ \quad +\alpha_x\left(B_1 \Delta f_{1,meas} + \Delta P_{tie\ 12,meas}\right) \end{array}\right] \\ &= S * \frac{B_1 K_{ps}}{T_{ps}}\left(\Delta P_{s,1}^{\cdot} - \Delta P_{L,1}^{\cdot} - \Delta P_{tie,12}^{\cdot}\right) - \frac{\Delta f_1^{\cdot}}{T_{ps}} + 2\pi T_{12}\left(\Delta f_1^{\cdot} - \Delta f_2^{\cdot}\right) + 2\pi T_{13}\left(\Delta f_1^{\cdot} - \Delta f_3^{\cdot}\right) \\ &\quad +\alpha_x\left(B_1 \Delta f_{1,meas}^{\cdot} + \Delta P_{tie\ 12,meas}^{\cdot}\right) \\ &= -\beta_c\left|S\right| < 0 \end{aligned}$$

Here, $\Delta f_1 = \Delta f_{1,meas}$, $\Delta P_{tie,12} = \Delta P_{tie,12}, meas\&\ \beta_c$ is a positive number. So, $V^{\cdot}$ is a negative definite function.

In this work, the proposed control law ($u_{sw,x}$) is having only switching law which has been given in Eq. (29).

$$u_{sw,x} = -k_{SMC,x} \times \mathrm{sgn}(S) \tag{29}$$

where, $\mathrm{sgn}(.)$ is a signum function and $k_{SMC,x}$ is a positive gain value designed tightly to diminish the error to zero.

The control signal produced by the Eq. (29) contains chattering. To mitigate these chattering, a saturation function is added into Eq. (30).

$$u_{sw\_sat,x} = -k_{SMC,x} \times \mathrm{sgn}(\lambda) \tag{30}$$

where, λ is given in Eq. (30).

$$\lambda = \begin{cases} 1 & S > \varphi_{upper} \\ \dfrac{S}{\varphi} & \varphi_{lower} < S < \varphi_{up} \\ -1 & S < \varphi_{lower} \end{cases} \tag{31}$$

where, $\varphi_{lower}\&\varphi_{upper}$ are the defined boundary limit in which the switching is carried out.

Both SMC and fuzzy logic controller work well independently as it has been introspected in the literature survey. But the flaws imbibing in each controller may put the system to performance inefficiently, e.g. the SMC controller produces chattering and improper membership function design in FL may cause sluggish response. So, to reap an efficient, prompt and noise-free response, the SMC controller has been conglomerated with FLC as shown in Fig. 5. Here, the controlled signal is composed of the signal produced by FLC and SMC controllers. The effective control law has been given in Eq. (32).

$$\begin{aligned} u_{FSMC,x} &= u_{sw\_sat,x} + u_{FLC} \\ &= -k_{SMC,x} \times \mathrm{sgn}(\lambda) + u_{FLC} \end{aligned} \tag{32}$$

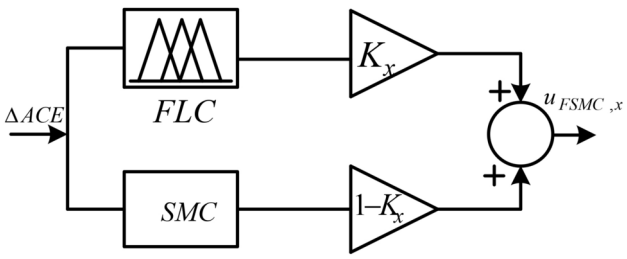

Fig. 5. Structure of fuzzy-SMC controller.

Here, u_{FLC} is the signal generated by FLC controller &λ is a saturation function as given in Eq. (31).

Gannet optimization algorithm (GOA)

GOA is a flock-based meta-heuristic algorithm[80] which is inspired by the extraordinary predatory ballet of the Northern Atlantic Gannet. These majestic sea birds, the largest to grace the northern Atlantic waters, boast slender neck and eyes that pierce the very depth of the ocean, for that it is very difficult for fish to escape from their eyes. The hunting strategy unfolds in two distinct stages i.e. Exploration and Exploitation. In the Exploration phase, the gannet embarks upon a quest to locate a suitable hunting ground once a promising region is found they plan for strategically dives like U-shaped and V-shaped. After that the ballet of exploitation commences, showcasing the gannet's remarkable capacity of capture. The details analysis of Exploration and Exploitation phases are listed below in the form of equations.

Like every optimization technique, GOA also starts with an initial phase, in which a solution matrix of size [NP, D] is randomly generated within the predefined search space using the relation:

$$X = X_{min} + (X_{max} - X_{min}) \times rand[NP, D] \tag{33}$$

Exploration Phase Gannets regulate their dive pattern into the water from the air as per the position of prey in the water. Generally, they follow two types of dive pattern namely (i) a U-shaded dive which is long and deep, or (ii) V-shaped dive which is short and shallow. These two dive patterns are mathematically modelled as follows:

$$a = 2\cos(2\pi r_1) \times t$$

$$b = 2 \times V(2\pi r_2) \times t$$

where, r_1 and r_2 are random numbers in the range [0, 1] and $t = 1 - \frac{iter}{itermax}$, iter is the current iteration number, itermax is the maximum number of iterations, and V(x) is given as:

$$V(x) = \begin{cases} \frac{-1}{\pi}x + 1 when x \in [0, \pi] \\ \frac{1}{\pi}x - 1 when x \in [\pi, 2\pi] \end{cases} \tag{34}$$

Gannets choose the V-shaped or U-shaped diving strategy with the same probability in order to catch their prey. So, the following equation is used to update the initial position of the gannets i.e. the initial population.

$$X_1 = \begin{cases} X + u_1 + u_2 if p \geq 0.5 \\ X + v_1 + v_2 if p < 0.5 \end{cases} \tag{35}$$

where, u1 (U-dives) and v1 (V-dives) are random numbers generated in the range [−a, +a] and [−b, +b] respectively, and u_2 and v_2 are calculated using the relations:

$$u_2 = A \times (X - X_r)$$

$$v_2 = B \times (X - X_m)$$

where,

$$A = 2 \times (r_3 - 1) \times a$$

$$B = 2 \times (r_4 - 1) \times b$$

X_r is a randomly selected probable solution and X_m is the mean position of the whole population and is given as:

$$X_m = \frac{1}{NP} \sum_{i=1}^{NP} X$$

Exploitation Phase In this phase, gannets spend lot of energy to capture the prey. Here the capturing capability i.e. capturability is calculated using the relation:

$$Capturability = \frac{1}{R \times T_2}$$

where, $T_2 = 1 + \frac{iter}{Itermax}$

$$R = \frac{M \times v}{L}$$

$$L = 0.2 + (2 - 0.2) \times r_5$$

where, M is the weight of the gannet which is taken as 2.5 kg, v is the velocity of the gannet which is taken as 1.5 m/s and r_5 is a random number taken in the range [0-1].

If the catching ability of the gannet is less than the capturability, the gannet updates its position by taking a levy flight to search for the next prey.

$$X_2 = \begin{cases} iter \times delta \times (X_1 - X_{best}) + X_1, & if\ Capturability \geq C \\ X_{best1} - (X_1 - X_{best1}) \times P \times iter & if\ Capturability < C \end{cases} \quad (36)$$

where,

$$delta = Capturability \times |X_1 - X_{best1}|$$

$$P = Levy = 0.01 \times \frac{\mu \times \sigma}{|v|^{\frac{1}{\beta}}}$$

$$\sigma = \left(\frac{\Gamma(1+\beta) \times sin\left(\frac{\pi\beta}{2}\right)}{\Gamma\left(\frac{1+\beta}{2}\right) \times \beta \times 2^{\left(\frac{\beta-1}{2}\right)}} \right)^{\frac{1}{\beta}}$$

C is taken as 0.2, μ and σ are random numbers in the range [0, 1] and β is taken as 1.5. X_{best1} is the best performing solution in X_1.

Modified GOA (MGOA)

In conventional mass of the gannet (M) and velocity (V) are taken as 2.5 kg and 1.5 m/s respectively. These two parameters play a very important role in the exploration phase of the GOA. So, in this article these two factors are optimally designed using the popular particle swarm optimization (PSO) technique[70] to improve the potential of the conventional GOA in exploration phase in searching/obtaining an improved solution. The range of mass of gannets and their velocity are taken as [1–4] kg and [0.5–3] m/s respectively.

PSO is a very simple and powerful algorithm having only two phases. Details regarding the implementation of PSO algorithm are explained below:

a. Initialization Phase: In this phase, initial population for the mass (M) and velocity (V) of gannets are randomly initialised in the range [1–4] and [0.5–3] respectively. Old velocity matrix for Mass (V_M^{old}) and velocity (M_V^{old}) of gannets are also generated randomly. Capturability of each gannet (i.e. each population of X_1 matrix obtained in Eq. (35) is calculated and the position is gannets are updated using the relation given in Eq. (36).
b. Updation Phase: In this phase, the mass and velocity of gannets are updated using the following relation:

$$M_V^{new} = w \times M_V^{old} + C_1 \times rand_1 \times (P_{bM} - M) + C_2 \times rand_2 \times (P_{gM} - M)$$

$$V_V^{new} = w \times V_V^{old} + C_1 \times rand_1 \times (P_{bV} - V) + C_2 \times rand_2 \times (P_{gV} - V)$$

$$M^{new} = M + M_V^{new} \quad (37)$$

$$V^{new} = V + V_V^{new} \quad (38)$$

Where, w decreases linearly from 0.9 to 0.4 with iteration count, C_1 & C_2 are taken as 2.05; $rand_1$ and $rand_2$ are random numbers in the range [0, 1], P_b & P_g are termed as local and global best.

After updation of gannet's mass and velocity, once again the capturability is calculated and the gannet's positions are updated using Eq. (36).

Pseudo code of the MGOA is given below:

Initialization Phase:

Randomly initialize the solution matrix X of size [NP, D] in the predefined search space using Eq. (33).

Exploration Phase:

Update the initial solution matrix X using Eq. (35).

Exploitation Phase:

Using PSO Algorithm initialize the mass of gannet (M) and their velocity (V), calculate the Capturability and update the population X_1 using Eq. (36).
Update the mass and velocity of the gannets and once again calculate the Capturability using the updated values of gannet's mass and velocity.
Once again update the position of gannets with the new Capturability using Eq. (36).

The performance of MGOA and GOA are tested with the help of 6 popular benchmark functions namely Booth (F1), Branin (F2), Griewank (F3), Matyas (F4), Powell (F5) and Rotated Hyper-Ellipsoid (F6). Detailed description of this benchmark function is indicated in Table 2. Performance of both MGOA, GOA and PSO algorithms are depicted in Fig. 6 and Table 3. From Fig. 6, it is clearly seen that in all the cases MGOA converges

Functions	Function's expression	Dimension	Range
Booth (F1)	$f_{Booth}(x) = (x_1 + 2x_2 - 7)^2 + (2x_1 + x_2 - 5)^2$	2	[– 10, 10]
Branin (F2)	$f_{Branin}(x) = a(x_2 - bx_1^2 + cx_1 - r)^2 + s.(1-t).\cos(x_1) + s$	2	[– 5, 0], [0–15]
Griewank (F3)	$f_{Griewank}(x) = \sum_{i=1}^{d} \frac{x_i^2}{4000} - \prod_{i=1}^{d} \cos\left(\frac{x_i}{\sqrt{i}}\right) + 1$	2	[– 600, 600]
Matyas (F4)	$f_{Matyas}(x) = 0.26.\left(x_1^2 + x_2^2\right) - 0.48x_1.x_2$	2	[– 10, 10]
Powell (F5)	$f_{Powell}(x) = \begin{bmatrix} (x_{4i-3} + 10.x_{4i-2})^2 + 5.(x_{4i-1} - x_{4i})^2 \\ + (x_{4i-2} - 2.x_{4i-1})^4 + 10.(x_{4i-3} - x_{4i})^4 \end{bmatrix}$	10	[– 4, 5]
Rotated hyper-ellipsoid (F6)	$f_{Rothyp}(x) = \sum_{i=1}^{d} \sum_{j=1}^{i} x_j^2$	30	[– 65.536, 65.536]

Table 2. Benchmark functions used to find the effectiveness of MGOA, GOA and PSO algorithms.

to their optimal values in less number of iterations. Table 3 also indicates that standard deviations of the optimal values of the benchmark functions are minimum with MGOA in comparison GOA & PSO. However computational time in MGOA is slightly more because of the inclusion of PSO algorithm in the exploration phase to determine the most suitable values of the masses of the gannets (M) and their velocities (v).

Result analysis

A three-area multi-sources system has been designed in MATLAB/SIMULINK 2016a environment as shown in Fig. 2. Further the system dynamics have been observed injecting EVs. Besides this, the impact of system non-linearities in the proposed model including EVs has been investigated. To regulate the system frequency different secondary controllers like PID, FPID, SMC and FSMC controllers have been designed endorsing GOA and MGOA optimization techniques. To have these optimal values, the algorithm has been run for fifty times. Also, the potential of the modified algorithm has been presented in the result section. Finally, the simulated results have been validated in OPAL-RT 4510 environment.

Simulation result analysis

Case 1: Transient Analysis without EVs

Performance under GOA optimization technique Under this condition we have considered three area multi-sources linearized model with a slip of 1% is applied in area-1 at the initial time to analyze the transient behavior. The gains of PID, FPID, SMC and FSMC are tuned with the conventional GOA technique has been provided in Table 4. The frequency variation (Δf) and tie-line power variation (Δp_{tie}) have been shown in Fig. 7 (i)-(vi). Performance parameters like undershoot (u_s), overshoot (o_s) and settling time (t_s) have been depicted in Table 5 for the respective cases. Here, the SMC controller has produced better result than PID and FPID controllers. Here, the FSMC controller has regulated the frequency deviation smoothly by eradicating oscillations and fast achieving steady state unlike the responses produced by PID, FPID & SMC controllers.

Performance under modified GOA optimization technique In this case, the proposed controllers have been designed by modifying GOA. The gain parameters have been given in Table 4. Keeping the same load variation as in the first case, the transient response of the system has been taken at time $t = 0$. The response of these controllers has been compared as presented in Fig. 8. The SMC controller has given better result in comparison to PID & FPID controllers, which is faster and incurring few cycles of oscillations with less amplitude. But, the FSMC controller has produced a staunch response which has achieved faster steady state with very minimal amplitude. This deviated quantity has been presented by the inset figure as shown in Fig. 8 (i)–(vi). The performance of these controllers has been given in Tables 5 and 6. Introspecting the data as in Tables 5 and 6, it is evident that the FSMC controller has performed well than other controllers.

Comparative study of proposed controller under GOA and MGOA technique Under this condition, a comparative study between conventional GOA-FSMC controller and MGOA-FSMC controller has been presented as shown in Fig. 9. The overshoot and response time are shorter for the modified GOA based FSMC controller as seen in the response curve. The settling time, overshoot and undershoot has been improved which is near about 90.52%, 62.18% and 74.35% respectively with the MGOA-FSMC controller in frequency variation of area-1 and about 85.75%,59.66% and 79.73% improvement has been observed in tie-line variation between area-1 and area-2. From, the analysis and performance parameters MGOA-FSMC controller have better response than conventional GOA.

Case 2: Transient analysis with Electric Vehicle (EV)

Without varying EV parameters Under this scenario, EV unit has been inserted in all three areas. The parameters of the EV for URC and DRC has been taken as 0.044pu and -0.096pu as per the work carried in[76]. The parameters of the secondary proposed FSMC controller are tuned with GOA and MGOA techniques and have been depicted in the Table 7. The dynamic behavior of the system with EV has been shown in the Fig. 10 (i)–(vi).

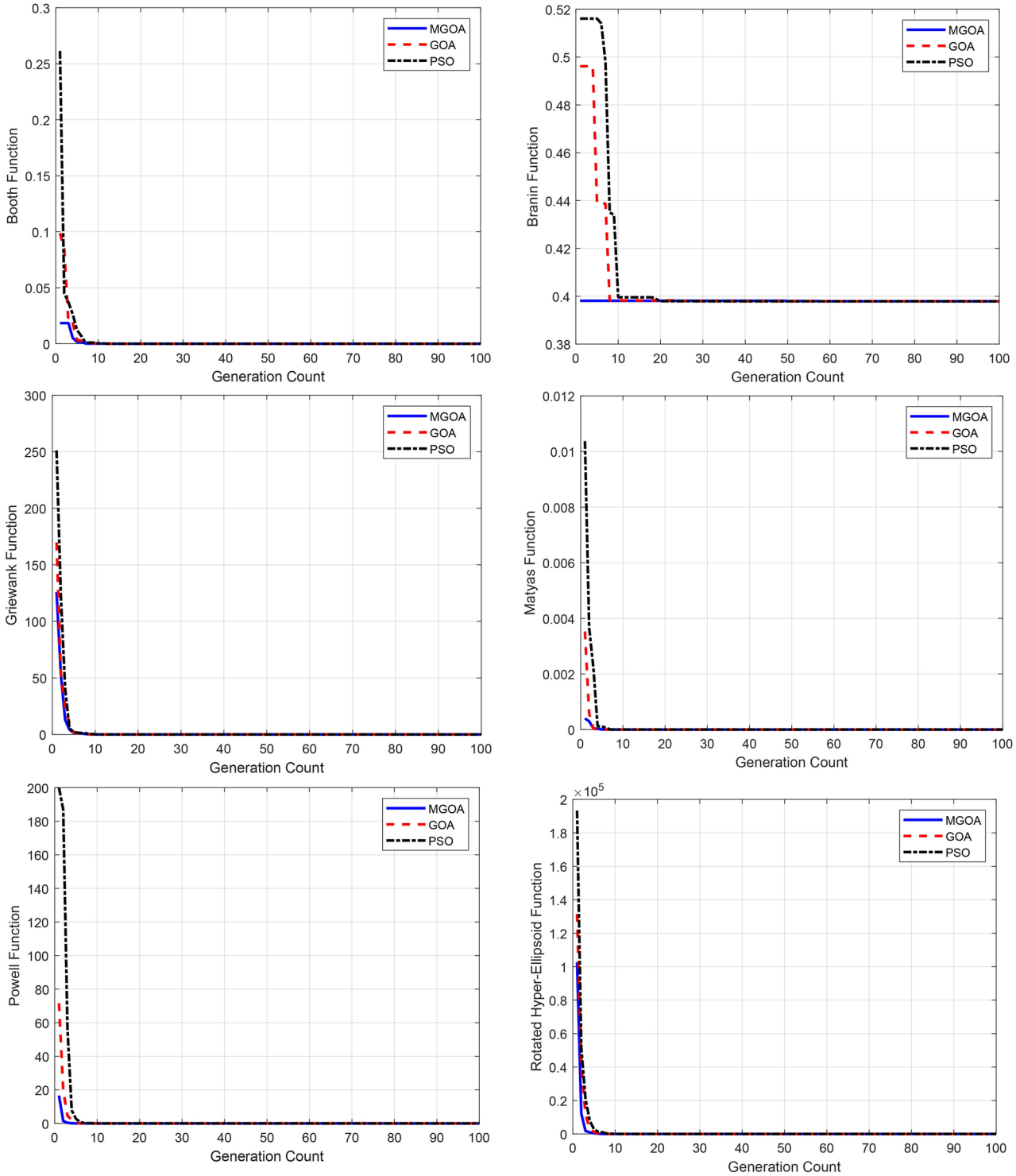

Fig. 6. Convergence curves of various functions.

The performance parameters have been tabulated in Table 8.The frequency deviations in all the three areas under MGOA-FSMC controller are 0.6129 mHz,0.6071 mHz and 0.6069 mHz respectively. So, the deviation is very insignificant as it does without the presence of EV. Hence, the proposed controller and the modified algorithm have a great potential to tackle the imbalanced caused by the integration of EV. Further, it has been observed that the MGOA-FSMC controller has ameliorated the frequency response nearly about 26.88%, 26.79% and 26.80%as compared to GOA-FSMC controller. Similarly, the power deviation has been improved well as noticed from the Fig. 10 and Table 8.

Algorithms	Functions	Optimum values	Minimum	Maximum	Mean value	Standard deviation	Computational time (s)
MGOA	F1	0	0	0	0	4.8457e−19	0.2394
GOA			0	0	0	7.4260e−17	0.1550
PSO			0	0	0	9.8825e−15	0.1325
MGOA	F2	0.397887	0.397887	0.397887	0.397887	1.8285e−09	0.2707
GOA			0.397887	0.397887	0.397887	3.8814e−07	0.1427
PSO			0.397887	0.397887	0.397887	5.8814e−06	0.1253
MGOA	F3	0	0	0	0	0	1.0123
GOA			0	0	0	0	0.8531
PSO			0	0	0	0	0.5692
MGOA	F4	0	0	0	0	3.3554e−67	0.2337
GOA			0	0	0	1.5917e−63	0.1321
PSO			0	0	0	5.6938e−59	0.0158
MGOA	F5	0	0	0	0	4.2722e−41	0.7871
GOA			0	0	0	1.1667e−37	0.5144
PSO			0	0	0	5.6897e−33	0.3257
MGOA	F6	0	0	0	0	7.6530e−67	0.5127
GOA			0	0	0	1.4939e−61	0.2105
PSO			0	0	0	3.2564e−57	0.1125

Table 3. Comparative performance of MGOA, GOA and PSO techniques.

With the variation of EV parameters Here, the parameters for up-regulation and down-regulation have been taken as mentioned in the Table 9. The dynamic response has been evaluated by applying GOA-FSMC & MGOA-FSMC controllers. The same controller gains have been set as used in the upper case. The MGOA-FSMC controller has improved the response curtailing the overshoots acutely as depicted in Fig. 11 (i)-(vi). The performance has been given in Table 10. The FSMC controller has performed robustly with this parameter variation. And also, the MGOA technique has a great capability to design the controller tightly so that the robust and stable performance of the controller has been achieved.

Case 3: Transient analysis with the inclusion of system non-linearities

Without varying EV parameters In this case, various non-linearities like GRC, GDB and boiler dynamics (BD) in the generating units have been included in the system as shown in Fig. 3. Also, EV has been integrated in the system with a fixed up and down regulation. Like other cases, 1% slip has been injected in area-1. The FSMC controller has been tuned by GOA and MGOA algorithms which have been amassed in Table 11. The time responses of the nonlinear system has been shown in the Fig. 12 (i)–(vi). And the performances have been tabulated in Table 12. From the response and the data in the table elucidates that the MGOA-FSMC controller has produced better result in comparison to the GOA-FSMC controller. The percentage of improvement of settling time, undershoot and overshoot of the proposed controller for frequency variation in area-1 and tie-line power variation between area-1 and area-2 are 26.05%, 12.69%, 13.97% and 28.28%, 20.19%, 47.87% respectively. Further, the dynamic response has been observed considering EV parameter variation as discussed in the next section.

With the variation of EV parameters Here, with this same test model, the up and down regulation as mentioned in the Table 9 have been included. Same designed parameters as used in the previous condition for the proposed controller have been set to evaluate the transient response of the system under non-linearities. The dynamic response has been given in Fig. 13 and the performance specifications have been tabled in Table 13. The frequency and tie-line power curves has shown that the MGOA-FSMC controller given an ameliorated response in comparison to GOA-FSMC controller. It is noteworthy that under such complexity, the proposed controller has tackled the perturbation eloquently and performed robustly. And the robust performance is possible due to the paramount tuning of the controller by the help of MGOA technique.

Case 4: System parameter variation In Case 4, system parameter variation, the deviation and standard deviation of area frequency are presented in Table 14, which quantifies the impact of system parameter variations on frequency stability. The data highlight how fluctuations in system parameters contribute to changes in area frequency, offering valuable insights into the sensitivity of the system's frequency response. Additionally, Table 15 shows the deviation and standard deviation of tie– line power under similar variations in system parameters. These results demonstrate how changes in the system's parameters influence the power exchange between interconnected areas, further contributing to a comprehensive understanding of system dynamics under varying conditions. Both tables provide essential metrics for evaluating the robustness and efficiency of the system in response to parameter fluctuations.

Controller	Optimization	Area controller	k_p	k_i	k_d	k_{p1}	k_{i1}	k_{pf}	k_{df}	x	y	z	k_{xi}
PID	GOA	x_1	0.4278	0.0012	1.2961								
		x_2	1.0103	1.7105	0.0126								
		x_3	0.1438	1.3245	0.0307								
		x_4	1.7145	0.6825	0.9771								
	MGOA	x_1	0.2728	0.0121	1.6144								
		x_2	1.0103	1.7105	0.0126								
		x_3	0.1438	1.3245	0.0307								
		x_4	1.7145	0.6825	0.9771								
FPID	GOA	x_1				1.0024	0.2018	0.3686	1.1819				
		x_2				0.2316	1.8793	0.2883	0.7878				
		x_3				0.4993	0.1516	1.7093	1.1934				
		x_4				1.1559	0.7102	1.7306	0.1445				
	MGOA	x_1				1.0224	0.1863	1.3686	1.8193				
		x_2				0.3167	1.8793	0.5883	0.8785				
		x_3				0.4993	0.1516	1.7093	1.1934				
		x_4				1.1559	0.7102	1.7306	0.1445				
SMC	GOA	x_1								10.8685	0.5161	− 1.7863	
		x_2								− 0.3530	− 7.9867	0.0184	
		x_3								5.8056	− 65.837	5.1727	
		x_4								− 1.7323	− 0.9550	− 3.3460	
	MGOA	x_1								25.0000	− 0.4826	3.9157	
		x_2								− 6.7545	− 4.9696	18.0000	
		x_3								− 3.2171	− 0.5606	− 2.3041	
		x_4								2.2932	18.000	− 15.414	
FSMC	GOA	x_1				0.9145	1.4585	1.8569	1.7444	1.8900	1.0430	3.2841	1.2103
		x_2				3.0074	2.8874	1.9839	3.2130	2.8735	1.0982	2.7414	0.5142
		x_3				12.8163	− 0.1355	15.6210	0.0100	4.4761	− 9.2510	5.7003	0.7868
		x_4				4.3366	5.2677	6.3544	5.4452	3.2824	8.6109	− 1.0597	0.6672
	MGOA	x_1				0.9145	1.4585	1.8569	1.7444	12.8163	− 0.1355	15.6218	0.4322
		x_2				1.8900	1.0430	3.2841	1.2103	11.2945	1.4051	13.8381	0.4503
		x_3				3.0074	2.8874	1.9839	3.2130	− 0.0433	2.3644	3.4765	0.2310
		x_4				2.8735	1.0982	2.7414	0.5142	− 6.3403	3.9957	16.0259	0.6735

Table 4. Optimal parameters of different controllers.

Hardware result analysis

The proposed model is executed in OPAL-RT to validate the result as observed in MATLAB/SIMULINK. The hardware set up has been provided in Fig. 14. Different cases like transient behavior under load deviation in an area, inclusion of EV and non-linearities in all areas have been studied. In the first case, different controller's performance designed by GOA algorithm has been analyzed against load perturbation. Further, to reap ameliorated response, MGOA has been considered. In the last case, system performance under FSMC controller designed by GOA and MGOA has been evaluated. The detailed study has been elaborated in the following sections.

Transient response of the system without EV GOA

In this case, the GOA based PID, FPID, SMC and FSMC controllers have been set in the proposed model to find the response with a load perturbation in area-1. The time division and voltage division of individual response have been illustrated in each figure as shown in Fig. 15. The FSMC controller has produced a significance response such that the frequency and tie-line deviation curves adhere the steady state faster with a meager steady state error.

Under MGOA based controllers

To improvise the dynamic response by eliminating the oscillations as incurred in the response presented in the last section, the MGOA based controllers have been incorporated. The excursion curves have been given in Fig. 16. Here, the PID, FPID and SMC controllers have curtailed the oscillations in frequency deviation as well as in tie-line power deviation curves significantly as compared to the curves observed in Fig. 16. The MGOA-FSMC controller has improved the response immensely as compared to the MGOA-SMC controller. It is evident from the response curve as in Fig. 16 that the MGOA-FSMC response settles faster with a minimal steady state error.

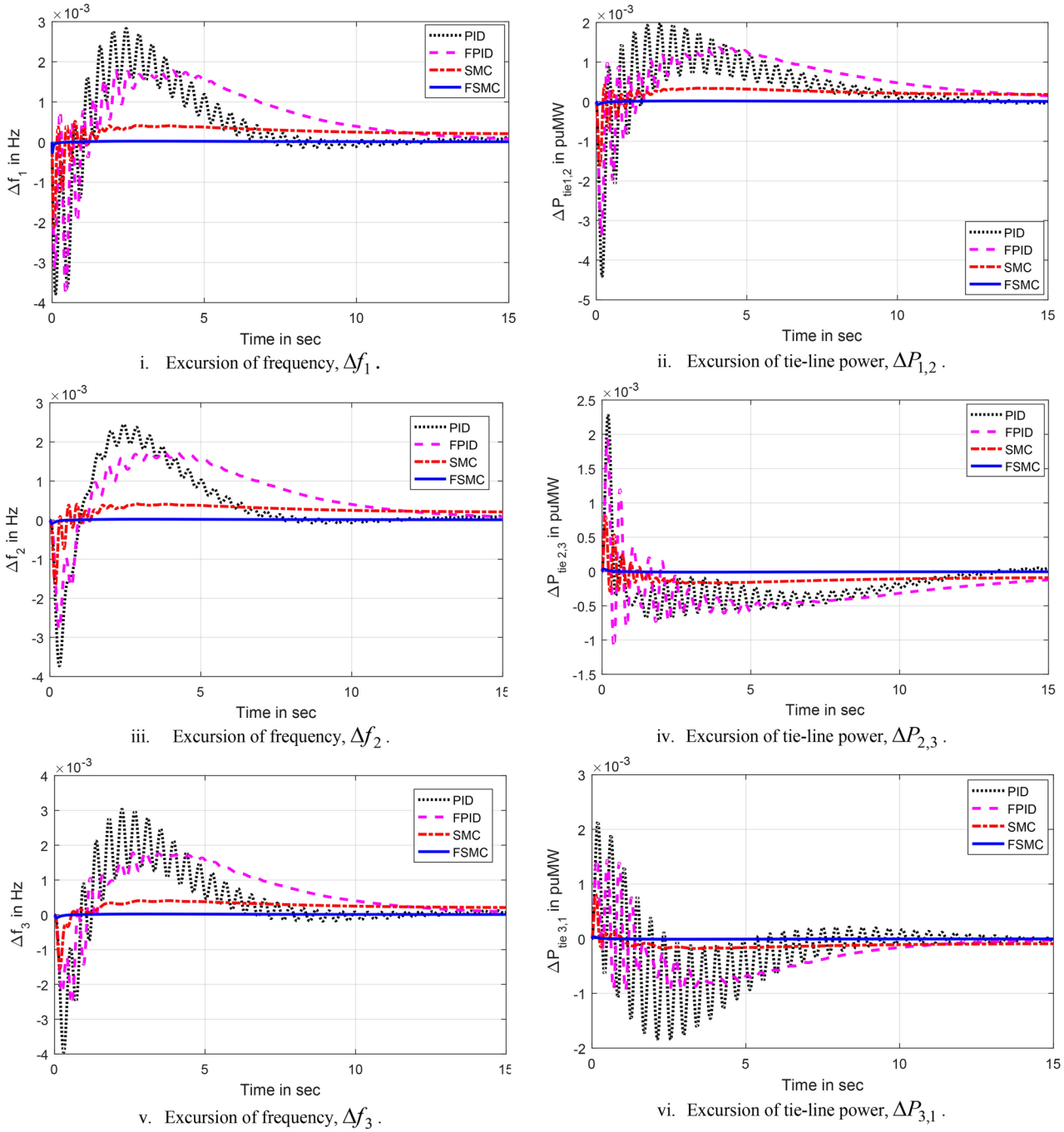

Fig. 7. Excursion of frequency and tie-line power.

Under EV and non-linearities

To investigate the robust performance of the SMC controller, different nonlinearities have been added into the test model. In addition to that EV units have been included with its parameter variation to that same system. The dynamic behavior of the system has been captured by OPAL-RT which has been shown in Fig. 17. Here, the response is similar to the response evaluated by MATLAM/SIMULINK as given Fig. 13. The MGOA-FSMC controller has ameliorated the response by curtailing its overshoots in system frequency as well as in tie-line powers. So, the FSMC controller has gained an upper hand over SMC controller to get better results. Simultaneously, the modified GOA has helped to produce better result than the GOA based SMC does.

Conclusion

An interconnected power system model of three areas has been executed in MATLAB/SIMULINK and real time simulator (OPAL-RT-4510) environment under different conditions. The inevitable outcomes of this work have been delineated as follows:

Controllers	Δf_1			Δf_2			Δf_3		
	$u_s \times 10^{-3}$ in Hz	$o_s \times 10^{-3}$ in Hz	t_s in sec	$u_s \times 10^{-3}$ in Hz	$o_s \times 10^{-3}$ in Hz	t_s in sec	$u_s \times 10^{-3}$ in Hz	$o_s \times 10^{-3}$ in Hz	t_s in sec
GOA-FSMC	− 0.8616	0.0595	4.46	− 0.2873	0.0572	0.14	− 0.2906	0.0571	0.14
MGOA-FSMC	− 0.2210	0.0225	0.423	− 0.0616	0.0225	7.90	− 0.0615	0.0225	7.90
GOA-SMC	− 2.1529	0.6204	0.08	− 1.7122	0.4969	12.23	− 1.5653	0.4046	12.22
MGOA-SMC	− 1.0137	0.4684	7.81	− 0.4299	0.1124	7.90	− 0.4958	0.1124	7.90
GOA-FPID	− 3.8053	1.7832	12.13	− 2.7884	1.7566	12.23	− 2.5676	1.8108	12.22
MGOA-FPID	− 2.6367	1.2542	7.81	− 2.0910	1.2563	7.90	− 1.8156	1.2245	7.90
GOA-PID	− 3.7588	2.7272	3.72	− 3.6894	2.4014	3.36	− 3.9092	2.8893	3.94
MGOA-PID	− 3.4846	2.2785	3.25	− 3.3349	2.2375	3.30	− 3.5036	2.3072	3.40

Table 5. Performance indices of different controllers.

i. The dynamic response produced by SMC controller over PID and FPID controllers is superior in the presence of DGs and EVs. And, the SMC controller has curtailed the overshoots and overshoots adequately with faster response.
ii. Anticipating the severe mismatch between load and generation due to intermittent uncertainties, non-linearities, and other external disturbances, the SMC controller has been restructured to intelligent FSMC controller. This FSMC controller has ameliorated the dynamic response splendidly that produced by the SMC controller.
iii. The FSMC controller has mitigated the frequency fluctuation adequately under parameter variation in EV and the proposed power system.
iv. From the transient response and performance indices, it is evident that the controller has been designed meticulously by the GOA algorithm.
v. Further, the modified GOA has improved the performance of the system appreciably in such a way that the robustness of the controller has been perceived.
vi. Concurrently, the convergence curve and the performance indices of the benchmark functions suggest that the MGOA has gained an upper hand to design these controllers tightly. Also, the MGOA algorithm is more efficient than the PSO algorithm as examined through benchmark functions.
vii. The real time simulator (OPAL-RT-4510) has produced an unequivocally exact response that the MATLAB simulation has produced. Here, it has been observed that the FSMC controller has achieved superior response in comparison to other SMC, FPID and PID controllers. Also, it can be underlined that the proposed GOA and MGOA algorithm have designed these controllers properly such that they are able to perform up the mark in real time simulator platform.

In future, the FSMC controller can be precious to employ in a power system to regulate the frequency under cyber-attack, multiple time varying communication delays etc. Further, the study of LFC employing FSMC can be extended to a micro-grid in which the occurrence of intermittent uncertainties is high and critical.

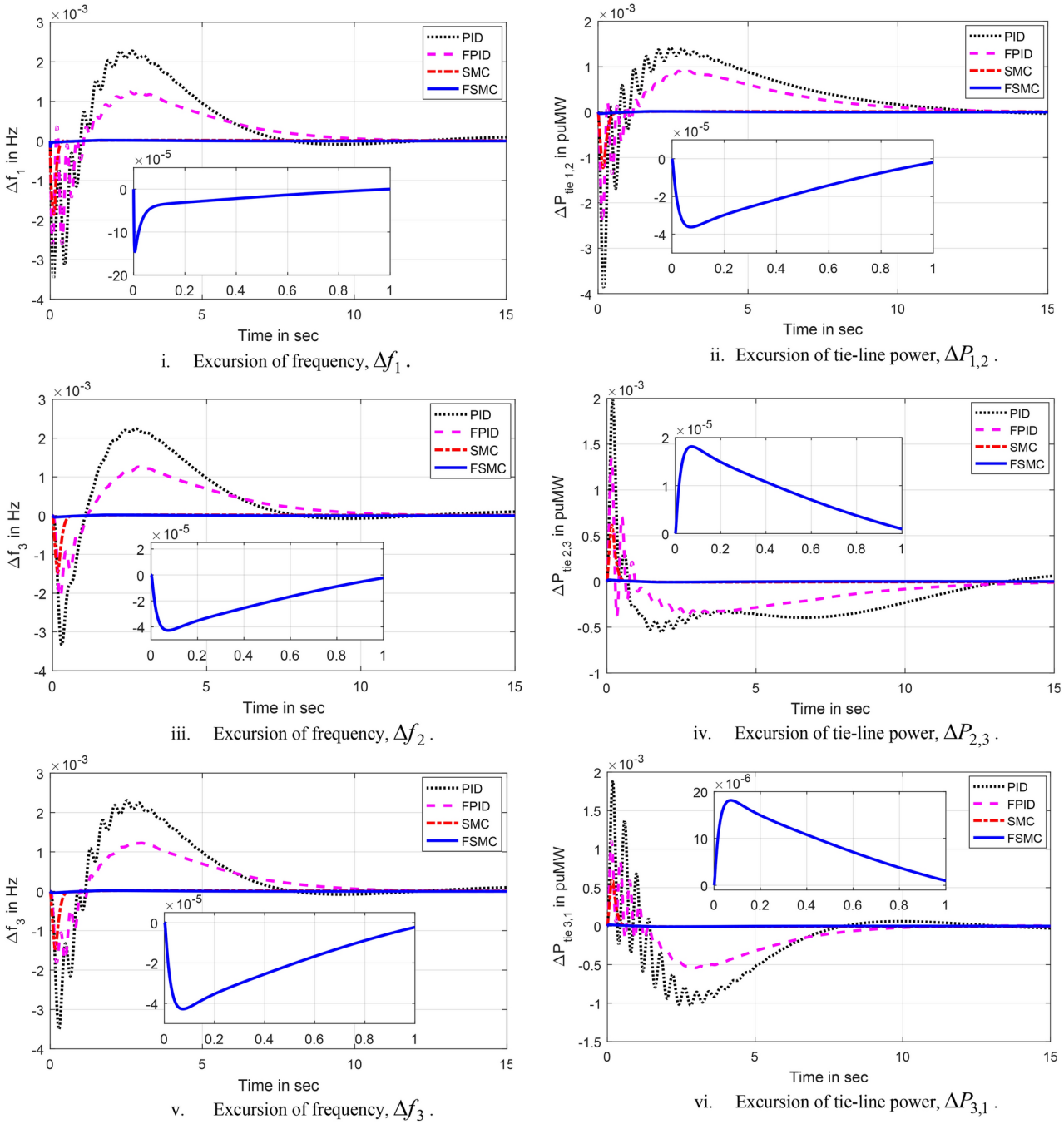

i. Excursion of frequency, Δf_1.

ii. Excursion of tie-line power, $\Delta P_{1,2}$.

iii. Excursion of frequency, Δf_2.

iv. Excursion of tie-line power, $\Delta P_{2,3}$.

v. Excursion of frequency, Δf_3.

vi. Excursion of tie-line power, $\Delta P_{3,1}$.

Fig. 8. Excursion of frequency and tie-line power in the system.

Controllers	$\Delta ptie_{12}$			$\Delta ptie_{23}$			$\Delta ptie_{31}$		
	$u_s \times 10^{-3}$ in puMW	$o_s \times 10^{-3}$ in puMW	t_s in sec	$u_s \times 10^{-3}$ in puMW	$o_s \times 10^{-3}$ in puMW	t_s in sec	$u_s \times 10^{-3}$ in puMW	$o_s \times 10^{-3}$ in puMW	t_s in sec
GOA-FSMC	− 0.2359	0.0476	3.22	− 0.0229	0.1185	12.60	− 0.0247	0.1174	9.32
MGOA-FSMC	− 0.0478	0.0192	0.459	− 0.0096	0.0241	6.94	− 0.0096	0.0237	6.14
GOA-SMC	− 1.6222	0.4644	13.77	− 0.3295	0.8061	12.60	− 0.1782	0.8161	9.32
MGOA-SMC	− 0.3946	0.0954	8.29	− 0.0475	0.1855	6.94	− 0.0560	0.2091	6.14
GOA-FPID	− 3.3630	1.3646	13.77	− 1.1086	1.9326	12.60	− 0.9525	1.4621	9.32
MGOA-FPID	− 2.4378	0.9044	8.29	− 0.3844	1.3450	6.94	− 0.5411	1.1037	6.14
GOA-PID	− 4.3555	1.8712	15.00	− 0.6752	2.2515	15.00	− 1.6799	2.1177	15.00
MGOA-PID	− 3.8657	1.4182	15.00	− 0.5534	1.9856	15.00	− 1.0278	1.8860	15.00

Table 6. Performance indices of different controllers.

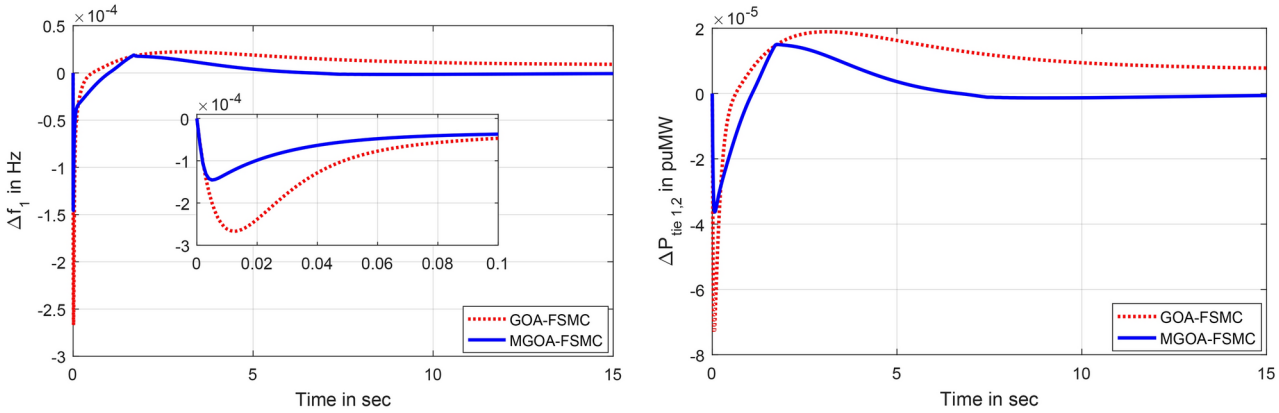

i. Excursion of frequency, Δf_1 .

ii. Excursion of tie-line power, $\Delta P_{1,2}$.

Fig. 9. Excursion of frequency and tie-line power in the system.

Controller	Optimization	Area controller	K_{p1}	K_{i1}	K_{pf}	K_{df}	x	y	z	K_{xi}
FSMC	GOA	x_1	9.0374	0.1943	1.5489	9.0000	− 7.6628	− 0.9867	0.3431	0.8000
		x_2	2.2906	6.6612	6.9924	0.8131	2.1200	− 9.0961	− 9.4435	0.8000
		x_3	0.0100	7.0000	3.4310	7.0000	− 5.4876	4.6952	− 5.5857	0.7411
		x_4	3.3289	5.9155	6.2604	0.3120	1.4998	− 3.4882	6.4911	0.6198
		x_5	6.1297	3.4270	7.0000	1.8337	− 9.5407	7.3619	− 0.5905	0.6984
	MGOA	x_1	9.0374	2.0943	1.5489	9.0000	− 7.6628	− 0.9867	0.3431	0.8000
		x_2	5.5290	6.6612	6.9924	0.8131	2.1200	− 9.0961	− 9.4435	0.8000
		x_3	0.0100	7.0000	3.4310	7.0000	− 5.4876	4.6952	− 5.5857	0.7411
		x_4	3.3289	5.9155	6.2604	0.3120	1.4998	− 3.4882	6.4911	0.6198
		x_5	6.1297	3.4270	7.0000	1.8337	− 9.5407	7.3619	− 0.5905	0.6984

Table 7. Optimal controller gains with EV.

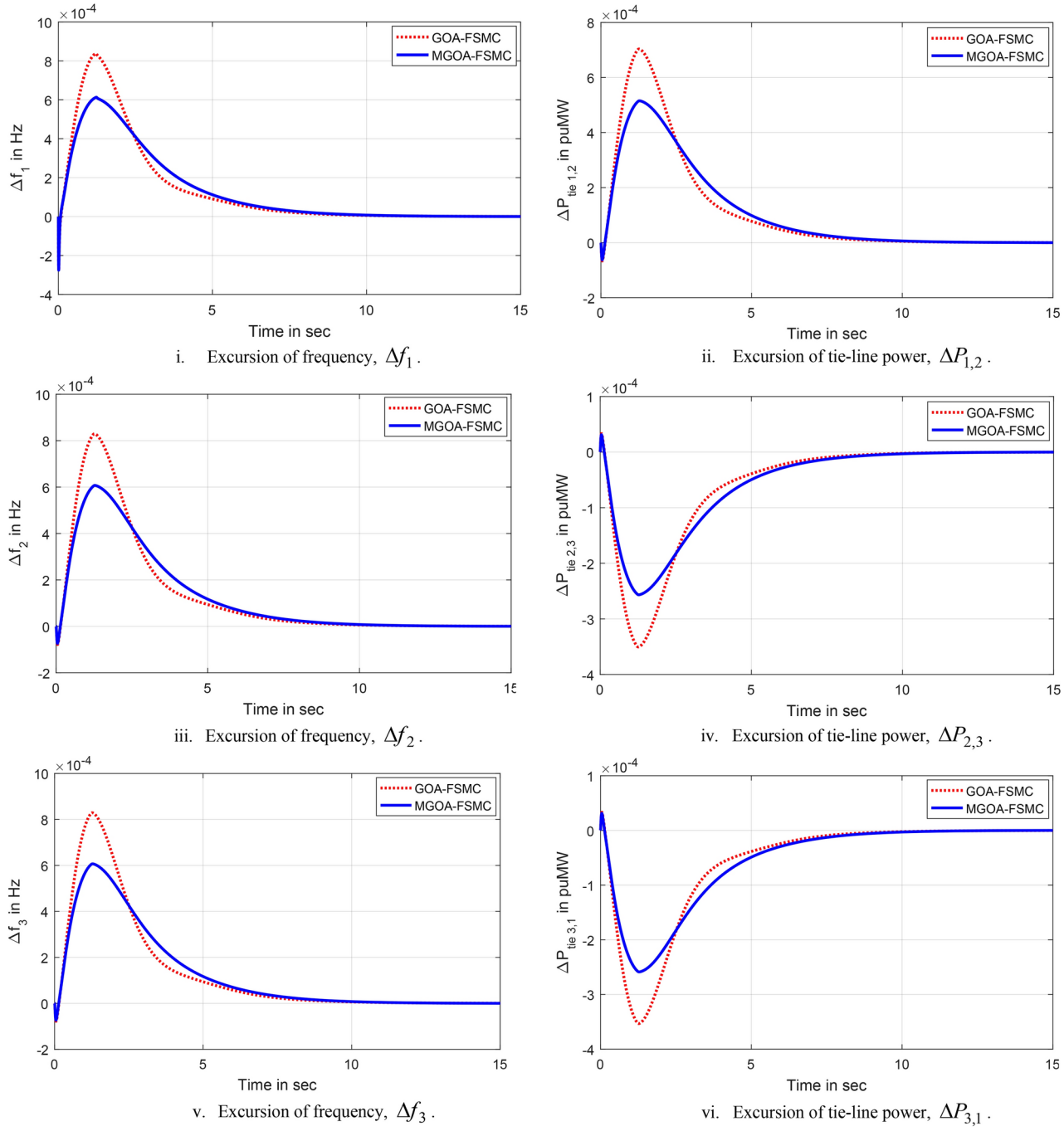

i. Excursion of frequency, Δf_1.

ii. Excursion of tie-line power, $\Delta P_{1,2}$.

iii. Excursion of frequency, Δf_2.

iv. Excursion of tie-line power, $\Delta P_{2,3}$.

v. Excursion of frequency, Δf_3.

vi. Excursion of tie-line power, $\Delta P_{3,1}$.

Fig. 10. Excursion of frequency and tie-line power.

Frequency deviation	Specification	GOA	MGOA	Tie-line power deviation	Specification	GOA	MGOA
Δf_1	$u_s \times 10^{-3}$ in Hz	− 0.2784	− 0.2751	$\Delta ptie_{12}$	$u_s \times 10^{-3}$ in puMW	− 0.0666	− 0.0625
	$o_s \times 10^{-3}$ in Hz	0.8378	0.6129		$o_s \times 10^{-3}$ in puMW	0.7037	0.5154
	t_s in sec	3.33	3.87		t_s in sec	3.23	3.68
Δf_2	$u_s \times 10^{-3}$ in Hz	− 0.0781	− 0.0733	$\Delta ptie_{23}$	$u_s \times 10^{-3}$ in puMW	− 0.3504	− 0.2566
	$o_s \times 10^{-3}$ in Hz	0.8293	0.6071		$o_s \times 10^{-3}$ in puMW	0.0334	0.0313
	t_s in sec	3.41	3.96		t_s in sec	2.39	2.29
Δf_3	$u_s \times 10^{-3}$ in Hz	− 0.0780	− 0.0732	$\Delta ptie_{31}$	$u_s \times 10^{-3}$ in puMW	− 0.3533	− 0.2588
	$o_s \times 10^{-3}$ in Hz	0.8291	0.6069		$o_s \times 10^{-3}$ in puMW	0.0333	0.0312
	t_s in sec	3.41	3.96		t_s in sec	2.40	2.30

Table 8. Performance parameters with EV.

Parameter (per unit)	Area-1	Area-2	Area-3
URC	0.044	0.067	0.056
DRC	− 0.096	− 0.143	− 0.119

Table 9. Parameters in URC and DRC[76].

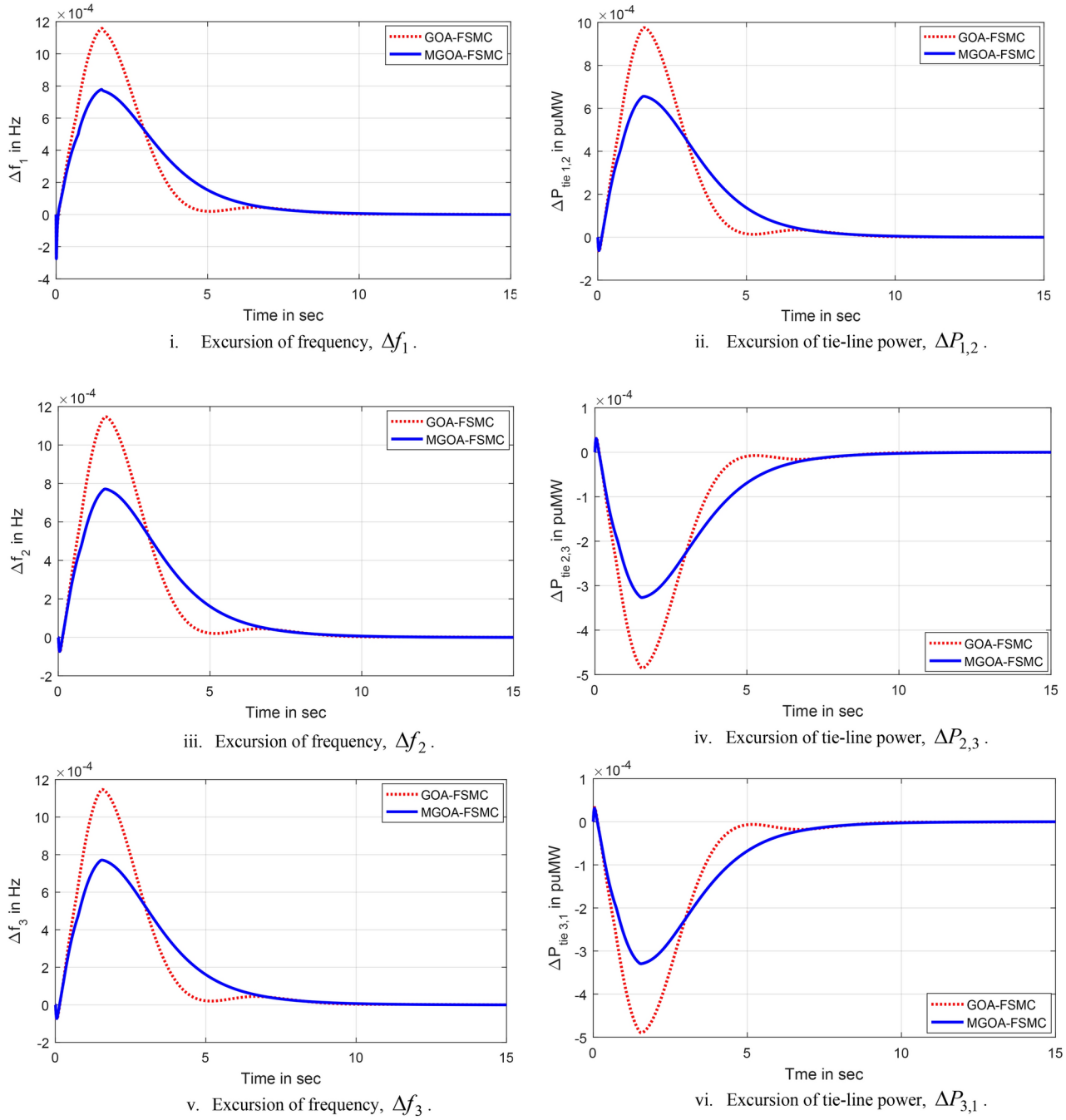

i. Excursion of frequency, Δf_1.

ii. Excursion of tie-line power, $\Delta P_{1,2}$.

iii. Excursion of frequency, Δf_2.

iv. Excursion of tie-line power, $\Delta P_{2,3}$.

v. Excursion of frequency, Δf_3.

vi. Excursion of tie-line power, $\Delta P_{3,1}$.

Fig. 11. Excursion of frequency and tie-line power.

Frequency deviation	Specification	GOA	MGOA	Tie-line power deviation	Specification	GOA	MGOA
Δf_1	$u_s \times 10^{-3}$ in Hz	− 0.2784	− 0.2751	$\Delta ptie_{12}$	$u_s \times 10^{-3}$ in puMW	− 0.0666	− 0.0625
	$o_s \times 10^{-3}$ in Hz	1.1582	0.7783		$o_s \times 10^{-3}$ in puMW	0.9752	0.6560
	t_s in sec	3.65	4.58		t_s in sec	3.65	4.43
Δf_2	$u_s \times 10^{-3}$ in Hz	− 0.0781	− 0.0733	$\Delta ptie_{23}$	$u_s \times 10^{-3}$ in puMW	− 0.4855	− 0.3266
	$o_s \times 10^{-3}$ in Hz	1.1472	0.7713		$o_s \times 10^{-3}$ in puMW	0.0334	0.0313
	t_s in sec	3.73	4.67		t_s in sec	3.11	3.25
Δf_3	$u_s \times 10^{-3}$ in Hz	− 0.0780	− 0.0732	$\Delta ptie_{31}$	$u_s \times 10^{-3}$ in puMW	− 0.4897	− 0.3294
	$o_s \times 10^{-3}$ in Hz	1.1470	0.7712		$o_s \times 10^{-3}$ in puMW	0.0333	0.0312
	t_s in sec	3.73	4.67		t_s in sec	3.10	3.23

Table 10. Performance parameters with EV parameter variation.

Controller	Optimization	Area controller	K_{p1}	K_{i1}	K_{pf}	K_{df}	x	y	z	K_{xi}
FSMC	GOA	x_1	5.0000	5.0000	5.0000	2.9525	− 7.2843	10.0000	6.1724	0.9000
		x_2	5.0000	5.0000	5.0000	4.0287	9.2608	6.2136	8.6596	0.9000
		x_3	5.0000	5.0000	5.0000	5.0000	− 4.4269	4.3559	10.0000	0.9000
		x_4	5.0000	5.0000	5.0000	1.1085	6.6710	8.7793	2.1738	0.9000
		x_5	5.0000	5.0000	2.5023	4.9034	9.9933	9.4321	− 1.1746	0.9000
	MGOA	x_1	10.000	8.0000	8.0000	4.2690	− 10.0000	10.0000	7.0407	0.9000
		x_2	9.0000	8.0000	7.0000	1.9933	7.2539	8.8113	8.8694	0.9000
		x_3	5.0000	5.0000	5.0000	5.0000	− 8.0371	5.8543	5.8765	0.9000
		x_4	5.0000	5.0000	5.0000	0.5619	8.6689	7.7820	0.9216	0.9000
		x_5	5.0000	5.0000	4.7668	4.9515	7.0476	10.0000	− 0.1861	0.9000

Table 11. Optimal controller gain with non-linearities under the presence of EV.

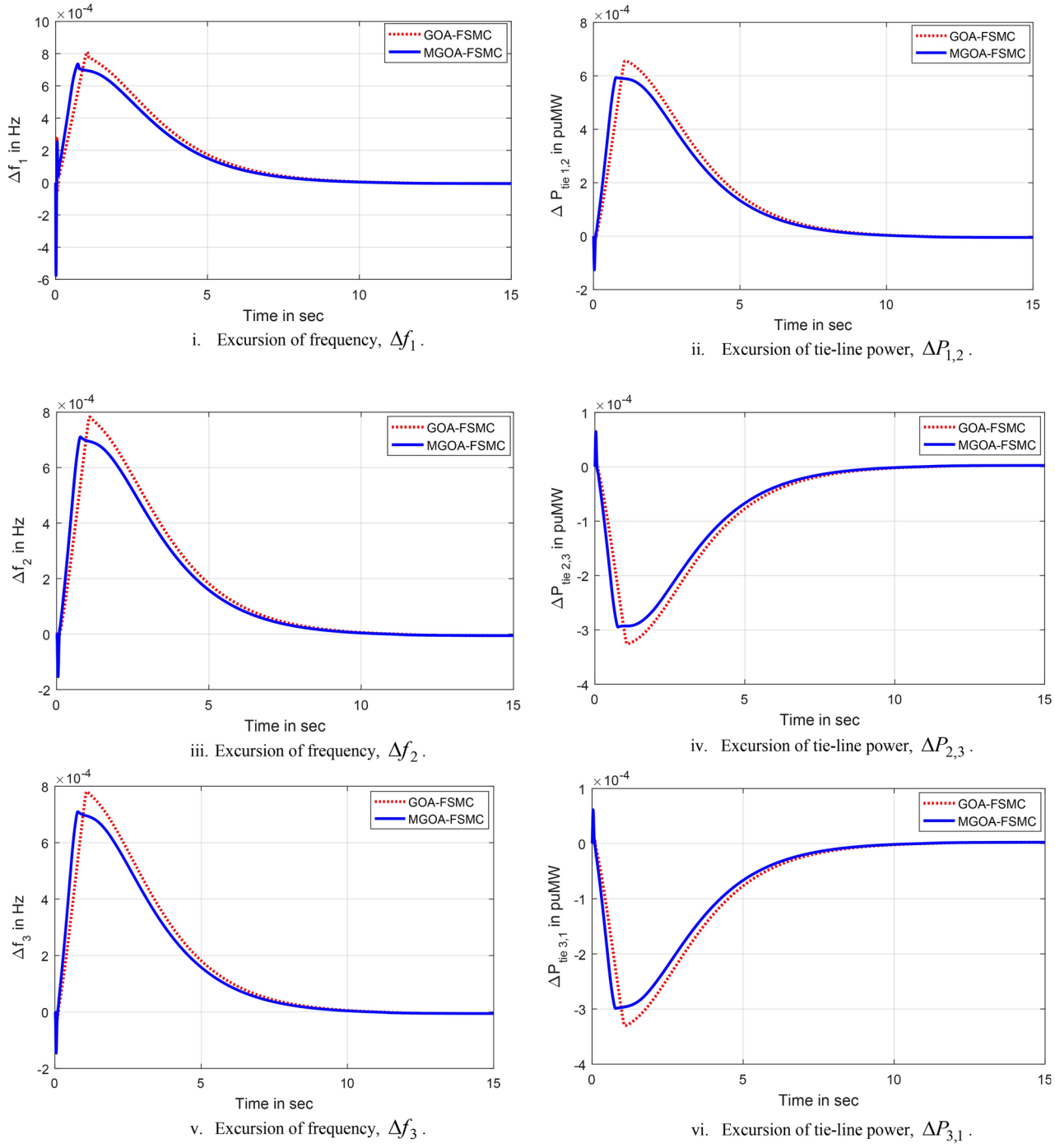

Fig. 12. Excursion of frequency and tie-line power in the system.

Frequency deviation	Specification	GOA	MGOA	Tie-line power deviation	Specification	GOA	MGOA
Δf_1	$u_s \times 10^{-3}$ in Hz	– 0.6631	– 0.5961	$\Delta ptie_{12}$	$u_s \times 10^{-3}$ in puMW	– 0.1419	– 0.1156
	$o_s \times 10^{-3}$ in Hz	0.8070	0.5482		$o_s \times 10^{-3}$ in puMW	0.6573	0.3394
	t_s in sec	4.73	3.49		t_s in sec	4.50	3.22
Δf_2	$u_s \times 10^{-3}$ in Hz	– 0.1774	– 0.1405	$\Delta ptie_{23}$	$u_s \times 10^{-3}$ in puMW	– 0.3270	– 0.1700
	$o_s \times 10^{-3}$ in Hz	0.7806	0.3919		$o_s \times 10^{-3}$ in puMW	0.0740	0.0590
	t_s in sec	4.81	3.57		t_s in sec	3.03	3.03
Δf_3	$u_s \times 10^{-3}$ in Hz	– 0.1709	– 0.1395	$\Delta ptie_{31}$	$u_s \times 10^{-3}$ in puMW	– 0.3303	– 0.1694
	$o_s \times 10^{-3}$ in Hz	0.7782	0.3920		$o_s \times 10^{-3}$ in puMW	0.0681	0.0565
	t_s in sec	4.81	3.57		t_s in sec	3.03	3.03

Table 12. Performance parameters with non-linearities under the presence of EV.

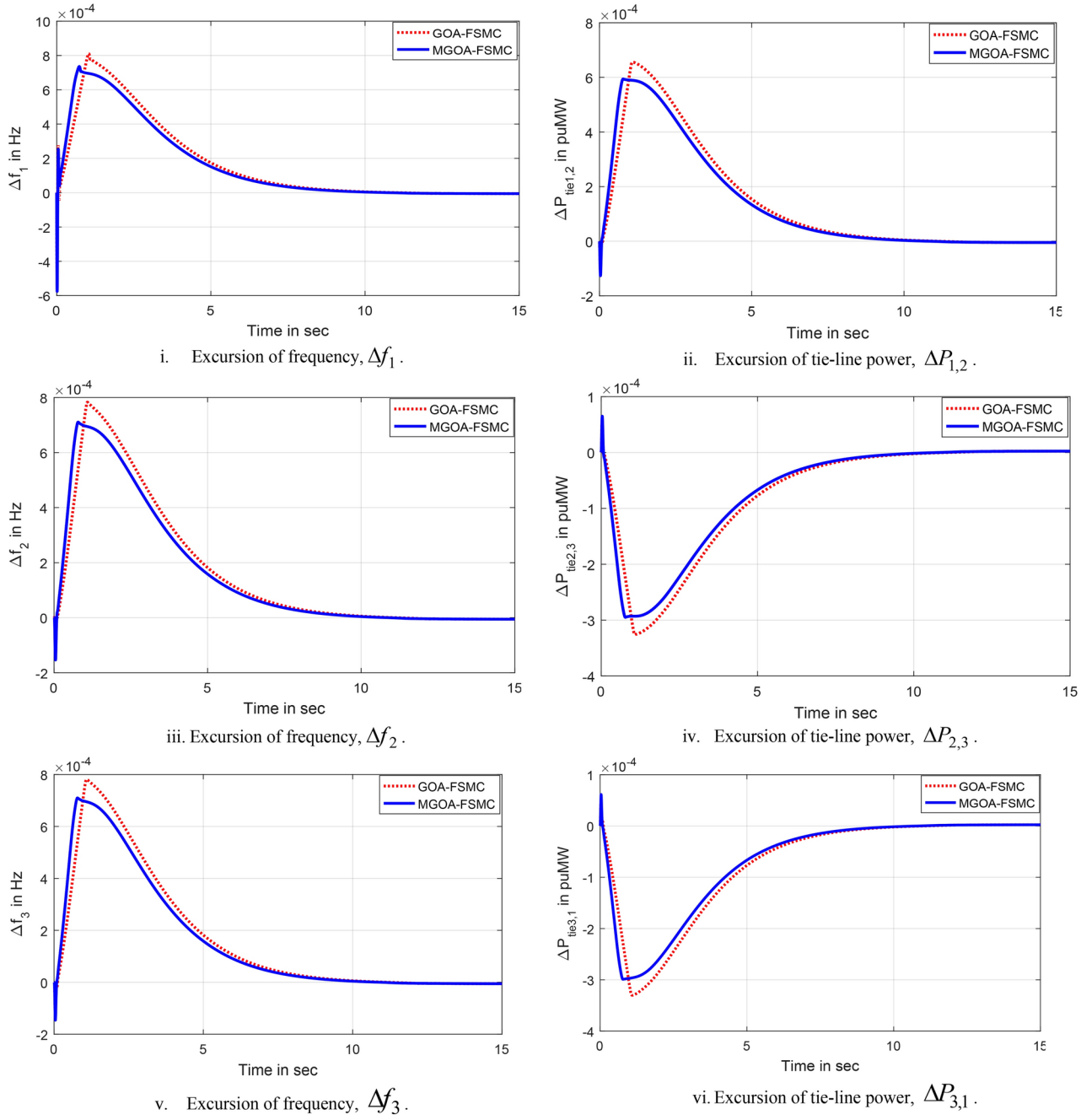

i. Excursion of frequency, Δf_1.

ii. Excursion of tie-line power, $\Delta P_{1,2}$.

iii. Excursion of frequency, Δf_2.

iv. Excursion of tie-line power, $\Delta P_{2,3}$.

v. Excursion of frequency, Δf_3.

vi. Excursion of tie-line power, $\Delta P_{3,1}$.

Fig. 13. Excursion of frequency and tie-line power in the system.

Frequency deviation	Specification	GOA	MGOA	Tie-line power deviation	Specification	GOA	MGOA
Δf_1	$u_s \times 10^{-3}$ in Hz	− 0.6631	− 0.5961	$\Delta ptie_{12}$	$u_s \times 10^{-3}$ in puMW	− 0.1419	− 0.1156
	$o_s \times 10^{-3}$ in Hz	0.8070	0.5482		$o_s \times 10^{-3}$ in puMW	0.6573	0.3394
	t_s in sec	4.73	3.49		t_s in sec	4.50	3.22
Δf_2	$u_s \times 10^{-3}$ in Hz	− 0.1774	− 0.1405	$\Delta ptie_{23}$	$u_s \times 10^{-3}$ in puMW	− 0.3270	− 0.1700
	$o_s \times 10^{-3}$ in Hz	0.7806	0.3919		$o_s \times 10^{-3}$ in puMW	0.0740	0.0590
	t_s in sec	4.81	3.57		t_s in sec	3.03	3.03
Δf_3	$u_s \times 10^{-3}$ in Hz	− 0.1709	− 0.1395	$\Delta ptie_{31}$	$u_s \times 10^{-3}$ in puMW	− 0.3303	− 0.1694
	$o_s \times 10^{-3}$ in Hz	0.7782	0.3920		$o_s \times 10^{-3}$ in puMW	0.0681	0.0565
	t_s in sec	4.81	3.57		t_s in sec	3.03	3.03

Table 13. Performance parameters with non-linearities under EV parameter variation.

Parameters	Variation in%	Δf_1			Δf_2			Δf_3		
		u_{sh}	o_{sh}	t_s	u_{sh}	o_{sh}	t_s	u_{sh}	o_{sh}	t_s
B	− 20	− 0.6293	0.7055	4.00	− 0.1819	0.5150	4.06	− 0.1814	0.5143	4.06
	− 10	− 0.6125	0.6575	3.73	− 0.1567	0.4445	3.81	− 0.1595	0.4445	3.81
	+ 10	− 0.5801	0.5186	3.28	− 0.1283	0.3603	3.37	− 0.1262	0.3604	3.37
	+ 20	− 0.5656	0.4884	3.07	− 0.1144	0.3278	3.16	− 0.1144	0.3279	3.16
R	− 20	− 0.5961	0.5484	3.49	− 0.1405	0.3913	3.57	− 0.1395	0.3913	3.57
	− 10	− 0.5961	0.5483	3.49	− 0.1405	0.3917	3.57	− 0.1395	0.3917	3.57
	+ 10	− 0.5961	0.5482	3.49	− 0.1405	0.3922	3.57	− 0.1395	0.3923	3.57
	+ 20	− 0.5961	0.5481	3.49	− 0.1405	0.3925	3.57	− 0.1395	0.3925	3.57
T_{12}	− 20	− 0.5992	0.4863	3.48	− 0.1168	0.3907	3.58	− 0.1178	0.3909	3.58
	− 10	− 0.5976	0.5180	3.48	− 0.1289	0.3907	3.57	− 0.1290	0.3908	3.57
	+ 10	− 0.5946	0.5771	3.50	− 0.1517	0.3965	3.57	− 0.1502	0.3963	3.57
	+ 20	− 0.5931	0.6045	3.51	− 0.1625	0.4031	3.58	− 0.1641	0.4028	3.58
K_{ps}	− 20	− 0.5060	0.5045	3.51	− 0.1229	0.4035	3.59	− 0.1219	0.4035	3.59
	− 10	− 0.5526	0.5674	3.50	− 0.1305	0.3966	3.58	− 0.1323	0.3967	3.58
	+ 10	− 0.6365	0.5974	3.49	− 0.1525	0.3939	3.57	− 0.1503	0.3940	3.57
	+ 20	− 0.6741	0.6460	3.49	− 0.1589	0.3932	3.57	− 0.1594	0.3933	3.57
T_{ps}	− 20	− 0.6918	0.6847	3.49	− 0.1651	0.3943	3.57	− 0.1630	0.3944	3.57
	− 10	− 0.6408	0.6018	3.50	− 0.1534	0.3980	3.58	− 0.1514	0.3979	3.58
	+ 10	− 0.5567	0.5731	3.50	− 0.1310	0.3979	3.58	− 0.1331	0.3980	3.58
	+ 20	− 0.5219	0.5272	3.51	− 0.1260	0.4006	3.59	− 0.1258	0.4006	3.59
Standard deviation		0.045021	0.06277	0.168273	0.017801	0.034463	0.163014	0.01769	0.034314	0.163014

Table 14. Deviation and standard deviation of area frequency under system parameter variation.

Parameters	Variation in%	$\Delta Ptie_{12}$			$\Delta Ptie_{23}$			$\Delta Ptie_{31}$		
		u_{sh}	o_{sh}	t_s	u_{sh}	o_{sh}	t_s	u_{sh}	o_{sh}	t_s
B	− 20	− 0.1318	0.3514	3.23	− 0.1757	0.0672	6.31	− 0.1757	0.0645	6.30
	− 10	− 0.1234	0.3454	3.23	− 0.1711	0.0630	6.31	− 0.1743	0.0604	6.30
	+ 10	− 0.1080	0.3366	3.22	− 0.1663	0.0552	6.31	− 0.1703	0.0529	6.30
	+ 20	− 0.1028	0.3363	3.22	− 0.1669	0.0520	6.31	− 0.1693	0.0508	6.30
R	− 20	− 0.1156	0.3397	3.22	− 0.1701	0.0590	6.30	− 0.1696	0.0565	6.30
	− 10	− 0.1156	0.3396	3.22	− 0.1701	0.0590	6.30	− 0.1695	0.0565	6.30
	+ 10	− 0.1156	0.3394	3.22	− 0.1700	0.0591	6.30	− 0.1694	0.0565	6.30
	+ 20	− 0.1156	0.3393	3.22	− 0.1700	0.0591	6.30	− 0.1694	0.0565	6.30
T_{12}	− 20	− 0.0957	0.3361	3.22	− 0.1681	0.0487	6.31	− 0.1680	0.0471	6.31
	− 10	− 0.1059	0.3373	3.22	− 0.1687	0.0540	6.31	− 0.1685	0.0519	6.30
	+ 10	− 0.1249	0.3403	3.21	− 0.1710	0.0640	6.30	− 0.1693	0.0609	6.30
	+ 20	− 0.1339	0.3417	3.22	− 0.1699	0.0687	6.31	− 0.1718	0.0651	6.29
K_{ps}	− 20	− 0.1089	0.3415	3.23	− 0.1691	0.0553	6.32	− 0.1725	0.0536	6.30
	− 10	− 0.1129	0.3410	3.22	− 0.1690	0.0575	6.31	− 0.1721	0.0554	6.30
	+ 10	− 0.1168	0.3392	3.22	− 0.1696	0.0598	6.30	− 0.1696	0.0576	6.30
	+ 20	− 0.1213	0.3377	3.21	− 0.1673	0.0616	6.31	− 0.1703	0.0597	6.30
T_{ps}	− 20	− 0.1233	0.3390	3.22	− 0.1685	0.0626	6.30	− 0.1705	0.0607	6.30
	− 10	− 0.1173	0.3381	3.22	− 0.1706	0.0598	6.31	− 0.1675	0.0579	6.30
	+ 10	− 0.1132	0.3410	3.23	− 0.1690	0.0577	6.31	− 0.1720	0.0555	6.30
	+ 20	− 0.1104	0.3429	3.23	− 0.1710	0.0562	6.31	− 0.1719	0.0543	6.30
Standard deviation		0.009283	0.003506	0.005871	0.001974	0.00483	0.005712	0.00206	0.004431	0.003244

Table 15. Deviation and standard deviation of tie-line power under system parameter variation.

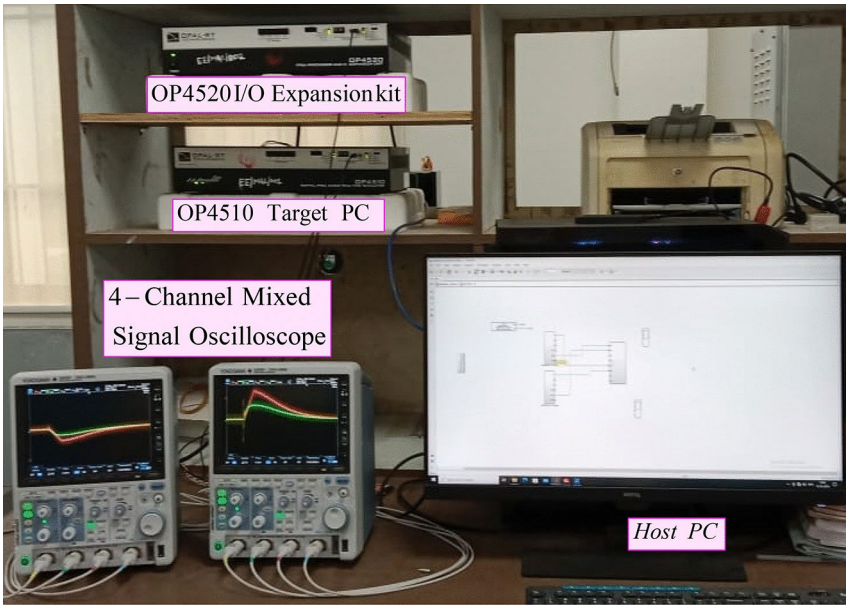

Fig. 14. OPAL-RT set up for the test model.

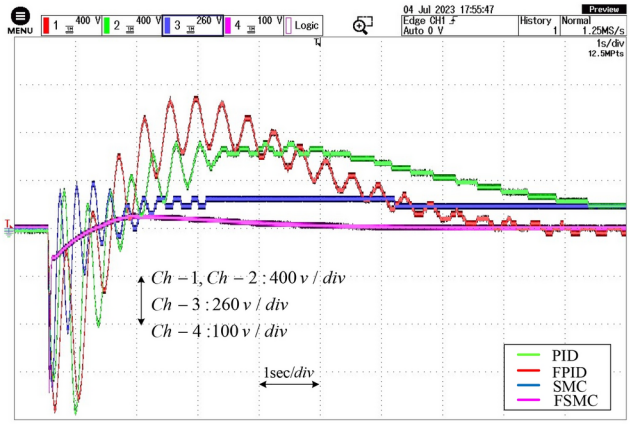

i. Frequency deviation, Δf_1 in area-1.

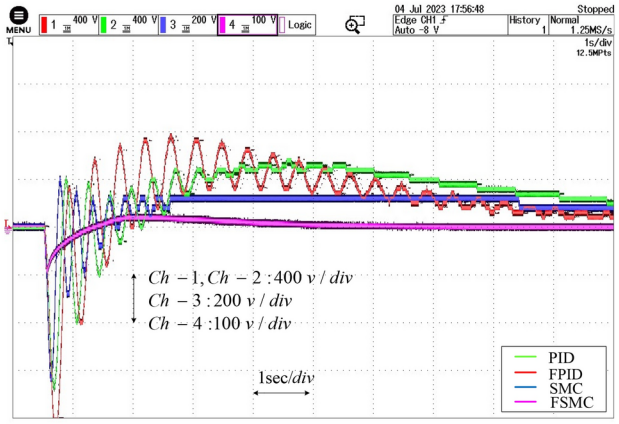

ii. Tie-line power deviation, $\Delta P_{1,2}$ in between area-1 & 2.

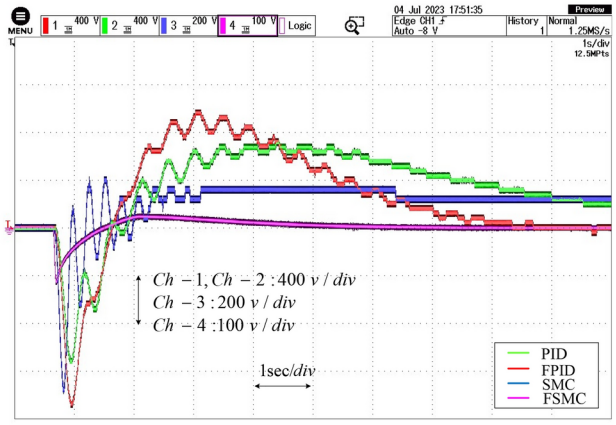

iii. Frequency deviation, Δf_2 in area-2.

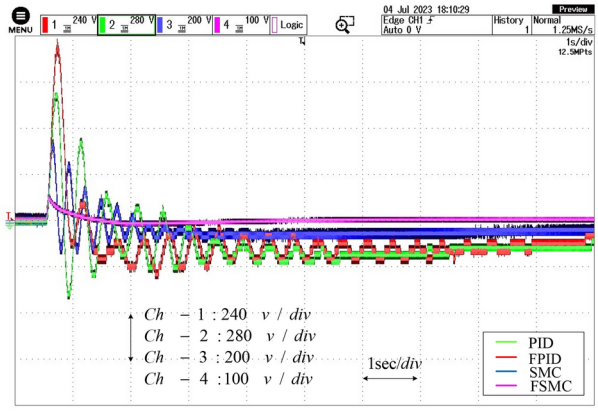

iv. Tie-line power deviation, $\Delta P_{2,3}$ in between area-2&3.

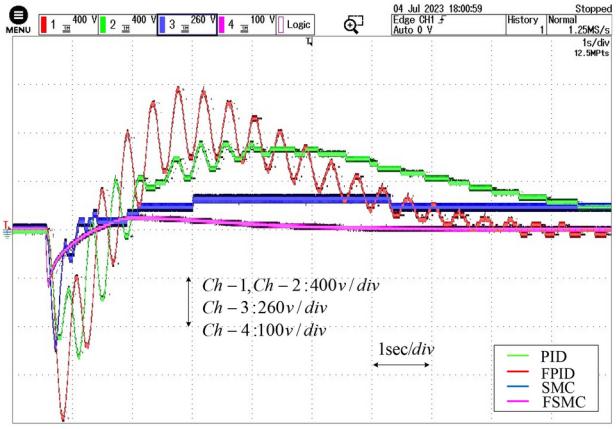

v. Frequency deviation, Δf_3 in area-3.

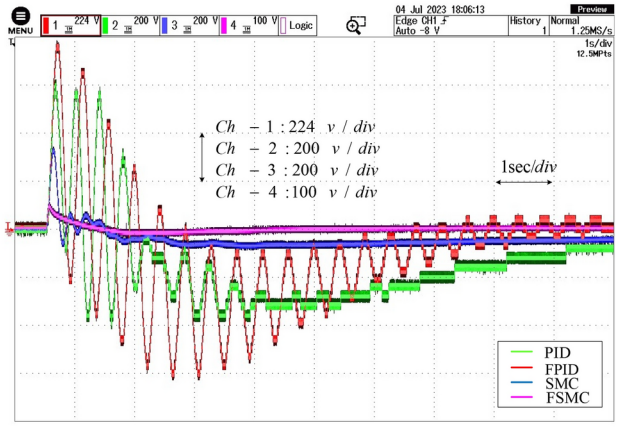

vi. Tie-line power deviation, $\Delta P_{3,1}$ in between area-3&1.

Fig. 15. Excursion of frequency and tie-line power in the system.

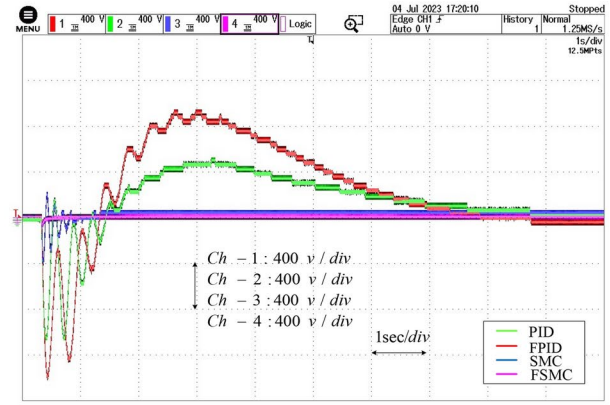

i. Frequency deviation, Δf_1 in area-1.

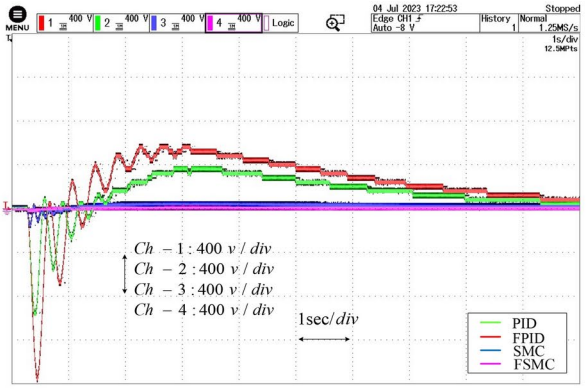

ii. Tie-line power deviation, $\Delta P_{1,2}$ in between area-1 & 2.

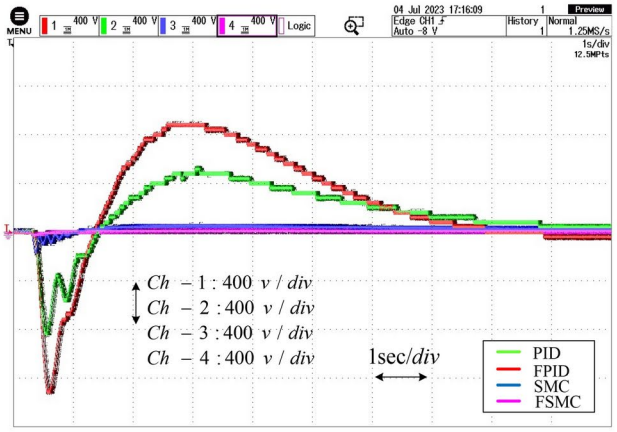

iii. Frequency deviation, Δf_2 in area-2.

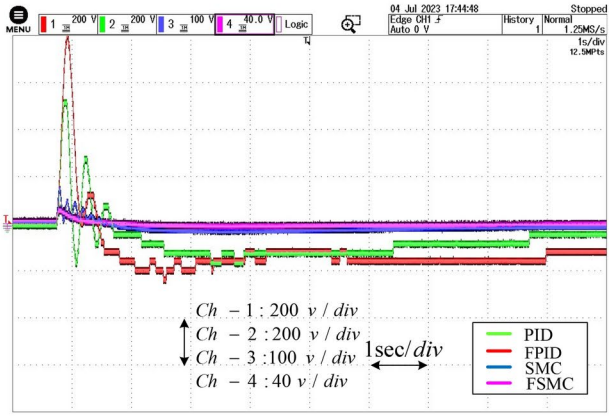

iv. Tie-line power deviation, $\Delta P_{2,3}$ in between area-2 & 3.

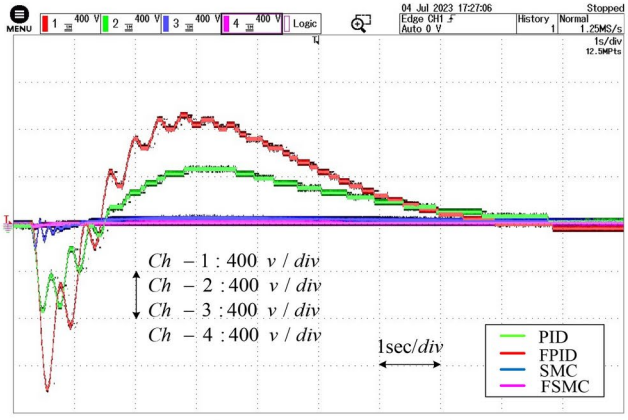

v. Frequency deviation, Δf_3 in area-3.

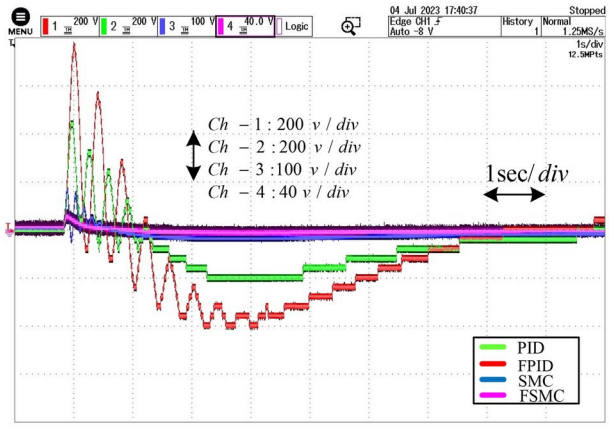

vi. Tie-line power deviation, $\Delta P_{3,1}$ in between area-3 & 1.

Fig. 16. Excursion of frequency and tie-line power in the system.

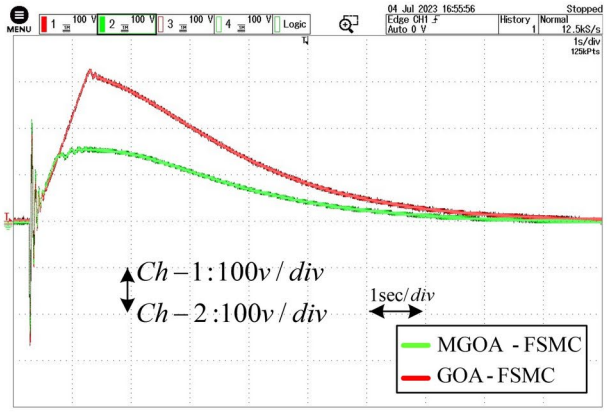

i. Frequency deviation curve in area-1.

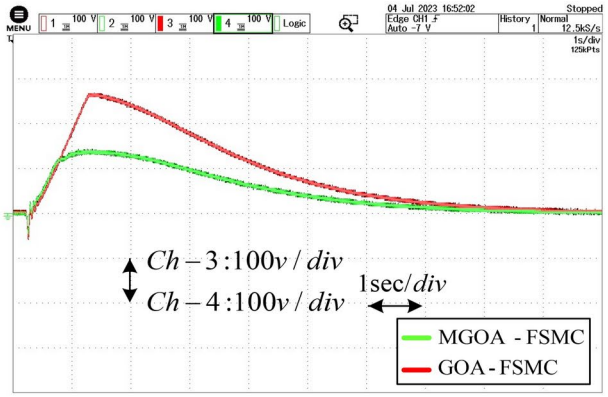

ii. Tie-line power deviation curve between area-1 & area-2.

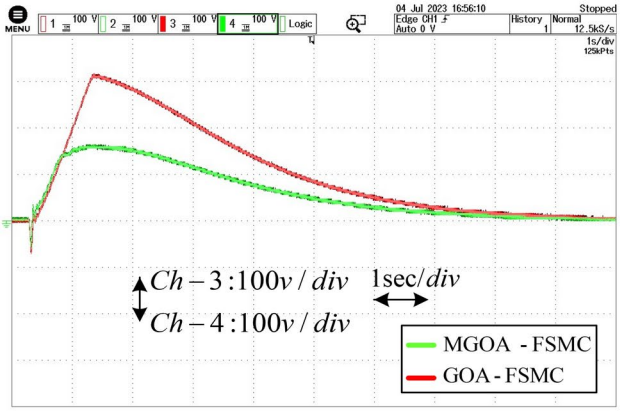

iii. Frequency deviation curve in area-2.

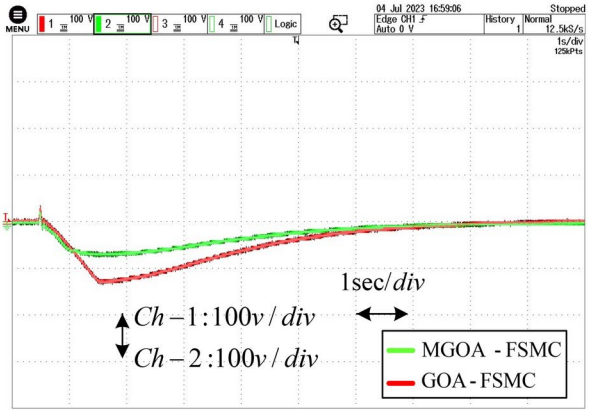

iv. Tie-line power deviation curve between area-2 & area-3.

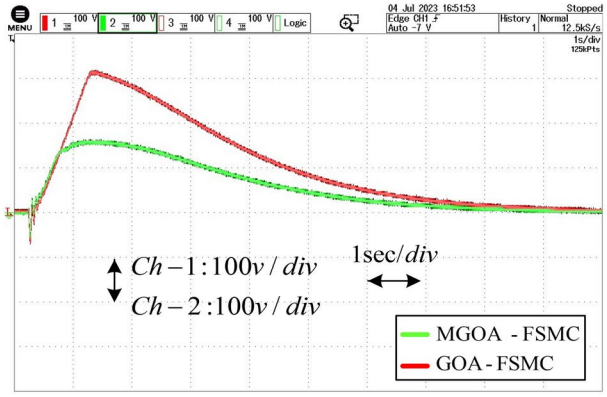

v. Frequency deviation curve in area-3.

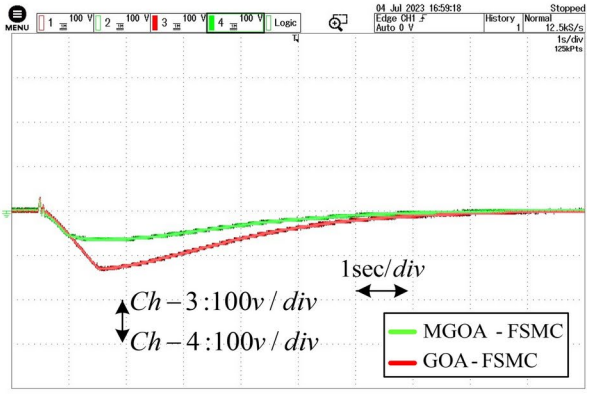

vi. Tie-line power deviation curve between area-3 & area-1.

Fig. 17. Excursion of frequency and tie-line power in the system.

Data availability

The datasets used and/or analysed during the current study available from the corresponding author on reasonable request.

Received: 26 November 2024; Accepted: 3 February 2025
Published online: 17 February 2025

References

1. Bevrani, H. et al. Power system frequency control: An updated review of current solutions and new challenges. *Electr. Power Syst. Res.* **194**, 107114 (2021).
2. Ranjan, M. & Shankar, R. A literature survey on load frequency control considering renewable energy integration in power system: Recent trends and future prospects. *J. Energy Storage* **45**, 103717 (2022).
3. Kundur, P. Power system stability. *Power Syst. Stab. Control* **10**, 7–1 (2007).

4. Kumar, P. & Kothari, D. P. Recent philosophies of automatic generation control strategies in power systems. *IEEE Trans. Power Syst.* **20**(1), 346–357 (2005).
5. Balachandran, P. K., Nwulu, N. & Babu, T. S. A perspective review of present and future trends of electric vehicle technology. *Renew. Energy Plug-In Electric Vehicles* 1–10 (2024).
6. Falahati, S., Taher, S. A. & Shahidehpour, M. Grid secondary frequency control by optimized fuzzy control of electric vehicles. *IEEE Trans. Smart Grid* **9**(6), 5613–5621 (2017).
7. Fan, H. et al. Frequency regulation of multi-area power systems with plug-in electric vehicles considering communication delays. *IET Gener. Transm. Distrib.* **10**(14), 3481–3491 (2016).
8. Gaur, P., Bhowmik, D. & Soren, N. Utilisation of plug-in electric vehicles for frequency regulation of multi-area thermal interconnected power system. *IET Energy Syst. Integr.* **1**(2), 88–96 (2019).
9. Arya, Y. Effect of electric vehicles on load frequency control in interconnected thermal and hydrothermal power systems utilising CF-FOIDF controller. *IET Gener. Transm. Distrib.* **14**(14), 2666–2675 (2020).
10. Ko, K. S. & Sung, D. K. The effect of EV aggregators with time-varying delays on the stability of a load frequency control system. *IEEE Trans. Power Syst.* **33**(1), 669–680 (2017).
11. Pappachen, A. & Fathima, A. P. Impact of SMES–TCSC combination in a multi-area deregulated power system with GA-based PI controller. *J. Control Autom. Electr. Syst.* **30**, 1069–1081 (2019).
12. Sahoo, S et al. Selfish Herd Optimisation tuned fractional order cascaded controllers for AGC analysis. *Soft Comput.* 1–19 (2022).
13. Nanda, J., Mishra, S. & Saikia, L. C. Maiden application of bacterial foraging-based optimization technique in multiarea automatic generation control. *IEEE Trans. Power Syst.* **24**(2), 602–609 (2009).
14. Das, D. C., Roy, A. K. & Sinha, N. GA based frequency controller for solar thermal–diesel–wind hybrid energy generation/energy storage system. *Int. J. Electr. Power Energy Syst.* **43**(1), 262–279 (2012).
15. Jena, N. K., Sahoo, S. & Sahu, B. K. Fractional order cascaded controller for AGC study in power system with PV and diesel generating units. *J. Interdiscip. Math.* **23**(2), 425–434 (2020).
16. Srilakshmi, K. et al. Multiobjective neuro-fuzzy controller design and selection of filter parameters of UPQC using predator prey firefly and enhanced harmony search optimization. *Int. Trans. Electr. Energy Syst.* **2024**(1), 6611240 (2024).
17. Kalyan, C. N. S. et al. Donkey and smuggler optimization algorithm-based degree of freedom controller for stability of two area power system with AC-DC links. In *2022 IEEE 7th International Conference on Recent Advances and Innovations in Engineering (ICRAIE)*, vol. 7 (IEEE, 2022).
18. Sahu, P. R. et al. Effective load frequency control of power system with two-degree freedom tilt-integral-derivative based on Whale Optimization Algorithm. *Sustainability* **15**(2), 1515 (2023).
19. Gorripotu, T. S., Priyadarshani, S. & Sahu, R. K. DE optimized TIDF controller for LFC of interconnected power system. 26–5 (2016).
20. Ahmed, M. et al. Modified TID controller for load frequency control of a two-area interconnected diverse-unit power system. *Int. J. Electr. Power Energy Syst.* **135**, 107528 (2022).
21. Guha, D., Roy, P. K. & Banerjee, S. Maiden application of SSA-optimised CC-TID controller for load frequency control of power systems. *IET Gener. Transm. Distrib.* **13**(7), 1110–1120 (2019).
22. Arya, Y. ICA assisted FTIλDN controller for AGC performance enrichment of interconnected reheat thermal power systems. *J. Ambient Intell. Human. Comput.* **14**(3), 1919–1935 (2023).
23. Jena, N. K. et al. Design of fractional order cascaded controller for AGC of a deregulated power system. *J. Control Autom. Electr. Syst.* **33**(5), 1389–1417 (2022).
24. Elaydi, H. & Wadi, M. Optimal controller for single area load frequency control via LQR and Legendre wavelet function. *J. Autom. Control* **3**(2), 43–47 (2015).
25. Ali, M. et al. Design of optimal linear quadratic gaussian (LQG) controller for load frequency control (LFC) using genetic algorithm (GA) in power system. *Int. J. Eng. Works* **5**(3), 40–49 (2018).
26. Alhelou, H. H., Golshan, M. E. H. & Hatziargyriou, N. D. Deterministic dynamic state estimation-based optimal LFC for interconnected power systems using unknown input observer. *IEEE Trans. Smart Grid* **11**(2), 1582–1592 (2019).
27. Biswas, J., Bera, P. & Chakrabarty, K. Determination of control area and design of fuzzy rule-tuned PID controller for LFC of multi-machine power system. *Electr. Power Syst. Res.* **221**, 109411 (2023).
28. Sahoo, S. et al. Self-adaptive fuzzy-PID controller for AGC study in deregulated Power System. *Indonesian J. Electr. Eng. Inform.* **7**(4), 650–663 (2019).
29. Kumari, N. et al. Dual degree branched type-2 fuzzy controller optimized with a hybrid algorithm for frequency regulation in a triple-area power system integrated with renewable sources. *Prot. Control Mod. Power Syst.* **8**(3), 1–29 (2023).
30. Wang, H. & Li, Z. S. Multi-area load frequency control in power system integrated with wind farms using fuzzy generalized predictive control method. *IEEE Trans. Reliab.* (2022).
31. Tian, E. & Peng, C. Memory-based event-triggering H∞ load frequency control for power systems under deception attacks. *IEEE Trans. Cybern.* **50**(11), 4610–4618 (2020).
32. Xiahou, K. S., Liu, Y. & Wu, Q. H. Robust load frequency control of power systems against random time-delay attacks. *IEEE Trans. Smart Grid* **12**(1), 909–911 (2020).
33. Shen, H. et al. An improved result on H∞ load frequency control for power systems with time delays. *IEEE Syst. J.* **15**(3), 3238–3248 (2020).
34. Shtessel, Y. et al. *Sliding Mode Control and Observation* Vol. 10 (Springer New York, 2014).
35. Utkin, V. et al. Conventional and high order sliding mode control. *J. Frankl. Inst.* **357**(15), 10244–10261 (2020).
36. Wang, Z. et al. Load frequency control of multi-region interconnected power systems with wind power and electric vehicles based on sliding mode control. *Energies* **14**(8), 2288 (2021).
37. Shouran, M., Anayi, F. & Packianather, M. The bees algorithm tuned sliding mode control for load frequency control in two-area power system. *Energies* **14**(18), 5701 (2021).
38. Jena, N. K. et al. Frequency stability analysis with fuzzy adaptive selfish herd optimization based optimal sliding mode controller for microgrids. *Int. J. Emerg. Electr. Power Syst.* **22**(5), 547–568 (2021).
39. Ansari, J., Abbasi, A. R. & Firouzi, B. B. Decentralized LMI-based event-triggered integral sliding mode LFC of power systems with disturbance observer. *Int. J. Electr. Power Energy Syst.* **138**, 107971 (2022).
40. Jabari, M. et al. A novel artificial intelligence based multistage controller for load frequency control in power systems. *Sci. Rep.* **14**(1), 29571 (2024).
41. Dev, A. et al. Enhancing load frequency control and automatic voltage regulation in Interconnected power systems using the Walrus optimization algorithm. *Sci. Rep.* **14**(1), 27839 (2024).
42. Daraz, A. et al. Frequency stabilization of interconnected diverse power systems with integration of renewable energies and energy storage systems. *Sci. Rep.* **14**(1), 25655 (2024).
43. Mahmoud, M. M. et al. Application of whale optimization algorithm based FOPI controllers for STATCOM and UPQC to mitigate harmonics and voltage instability in modern distribution power grids. *Axioms* **12**(5), 420 (2023).
44. Ardjoun, S. A. E. M., Denaï, M. & Chafouk, H. A robust control approach for frequency support capability of grid-tie photovoltaic systems. *J. Solar Energy Eng.* **145**(2), 021009 (2023).
45. Davoudkhani, I. F. et al. Maiden application of mountaineering team-based optimization algorithm optimized 1PD-PI controller for load frequency control in islanded microgrid with renewable energy sources. *Sci. Rep.* **14**(1), 22851 (2024).

46. Ekinci, S. et al. Frequency regulation of PV-reheat thermal power system via a novel hybrid educational competition optimizer with pattern search and cascaded PDN-PI controller. *Results Eng.* **24**, 102958 (2024).
47. Gopi, P. et al. Improving load frequency controller tuning with rat swarm optimization and porpoising feature detection for enhanced power system stability. *Sci. Rep.* **14**(1), 15209 (2024).
48. Davoudkhani, I. F. et al. Robust load-frequency control of islanded urban microgrid using 1PD-3DOF-PID controller including mobile EV energy storage. *Sci. Rep.* **14**(1), 13962 (2024).
49. Daraz, A. et al. Load frequency stabilization of distinct hybrid conventional and renewable power systems incorporated with electrical vehicles and capacitive energy storage. *Sci. Rep.* **14**(1), 9400 (2024).
50. Begum, B. et al. Application of an intelligent fuzzy logic based sliding mode controller for frequency stability analysis in a deregulated power system using OPAL-RT platform. *Energy Rep.* **11**, 510–534 (2024).
51. Daraz, A. et al. Frequency regulation of interconnected hybrid power system with assimilation of electrical vehicles. *Heliyon*. **10**(6) (2024).
52. Kalyan, C. H. N. S. et al. Frequency regulation of geothermal power plant-integrated realistic power system with 3DOFPID controller. *Cogent Eng.* **11**(1), 2322820 (2024).
53. Kalyan, C. H. N. S. et al. Water cycle algorithm optimized type II fuzzy controller for load frequency control of a multi-area, multi-fuel system with communication time delays. *Energies* **14**(17), 5387 (2021).
54. Dunna, V. K. et al. Super-twisting MPPT control for grid-connected PV/battery system using higher order sliding mode observer. *Sci. Rep.* **14**(1), 16597 (2024).
55. Izci, D., Abualigah, L., Can, Ö., Andiç, C. & Ekinci, S. Achieving improved stability for automatic voltage regulation with fractional-order PID plus double-derivative controller and mountain gazelle optimizer. *Int. J. Dyn. Control.* 1–6 (2024).
56. Aribowo, W., Abualigah, L., Oliva, D. & Prapanca, A. A novel modified mountain gazelle optimizer for tuning parameter proportional integral derivative of DC motor. *Bull. Electr. Eng. Inform.* **13**(2), 745–752 (2024).
57. Widi, A. et al. Controlling parameters proportional integral derivative of DC motor using a gradient-based optimizer. *Int. J. Power Electron. Drive Syst.* **15**(2), 696–703 (2024).
58. Premkumar, M. et al. Optimal operation and control of hybrid power systems with stochastic renewables and FACTS devices: An intelligent multi-objective optimization approach. *Alex. Eng. J.* **93**, 90–113 (2024).
59. Pandya, S. B. et al. Multi-objective RIME algorithm-based techno economic analysis for security constraints load dispatch and power flow including uncertainties model of hybrid power systems. *Energy Rep.* **11**, 4423–4451 (2024).
60. Alsmadi, O., Abu-Hammour, Z. & Mahafzah, K. Digital systems model order reduction with substructure preservation and fuzzy logic control. *Eurasia Proc. Sci. Technol. Eng. Math.* **28**, 14–22 (2024).
61. Abualigah, L., Ekinci, S. & Izci, D. Aircraft pitch control via filtered proportional-integral-derivative controller design using sinh cosh optimizer. *Int. J. Robot. Control Syst.* **4**(2), 746–757 (2024).
62. Alrashed, M. M., Flah, A., Dashtdar, M., El-Bayeh, C. Z. & Elnaggar, M. F. Improving the control strategy of the DVR compensator based on an adaptive notch filter with an optimized PD controller using the IGWO algorithm. *Int. Trans. Electr. Energy Syst.* **2024**(1), 5097056 (2024).
63. Fadheel, B. A. et al. A hybrid sparrow search optimized fractional virtual inertia control for frequency regulation of multi-microgrid system. *IEEE Access*. (2024).
64. Abualigah, L., Izci, D., Ekinci, S. & Zitar, R. A. Optimizing aircraft pitch control systems: a novel approach integrating artificial rabbits optimizer with PID-F controller. *Int. J. Robot. Control Syst.* **4**(1), 354–364 (2024).
65. Izci, D. et al. Refined sinh cosh optimizer tuned controller design for enhanced stability of automatic voltage regulation. *Electr. Eng.* 1–4 (2024).
66. Izci, D. et al. A novel control scheme for automatic voltage regulator using novel modified artificial rabbits optimizer. *E-Prime-Adv. Electr. Eng. Electron. Energy.* **6**, 100325 (2023).
67. Altawil, I. et al. Optimization of fractional order PI controller to regulate grid voltage connected photovoltaic system based on slap swarm algorithm. *Int. J. Power Electron. Drive Syst.* **14**, 1184–1200 (2023).
68. Abualigah, L., Ekinci, S., Izci, D. & Zitar, R. A. Modified elite opposition-based artificial hummingbird algorithm for designing FOPID controlled cruise control system. *Intell. Autom. Soft Comput.* **38**(2) (2023).
69. Sarayrah, A., Haj-ahmed, M. A. & Feilat, E. A. A study of a damping control based predictive strategy on an inter-area power system. In *2023 IEEE PES GTD International Conference and Exposition (GTD)*, 60–66 (IEEE, 2023).
70. Kennedy, J. The particle swarm: social adaptation of knowledge. In *Proceedings of 1997 IEEE International Conference on Evolutionary Computation (ICEC'97)* (IEEE, 1997).
71. Raj, U. & Shankar, R. Deregulated automatic generation control using novel opposition-based interactive search algorithm cascade controller including distributed generation and electric vehicle. *Iran. J. Sci. Technol. Trans. Electr. Eng.* **44**, 1233–1251 (2020).
72. Aljafari, B. et al. Solar photovoltaic converter controller using opposition-based reinforcement learning with butterfly optimization algorithm under partial shading conditions. *Environ. Sci. Pollut. Res.* **30**(28), 72617–72640 (2023).
73. Jiang, L. et al. Delay-dependent stability for load frequency control with constant and time-varying delays. *IEEE Trans. Power Syst.* **27**(2), 932–941 (2011).
74. VikramGoud, M. et al. Advancement of electric vehicle technologies, classification of charging methodologies, and optimization strategies for sustainable development-a comprehensive review. *Heliyon*. (2024).
75. Babu, T. S., Balachandran, P. K. & Nwulu, N. *Renewable Energy for Plug-In Electric Vehicles: Challenges, Approaches, and Solutions for Grid Integration*. (2024).
76. Khan, M. et al. Electric vehicles participation in load frequency control based on mixed H2/H∞. *Int. J. Electr. Power Energy Syst.* **125**, 106420 (2021).
77. Utkin, V., Guldner, J. & Shijun, M. *Sliding Mode Control in Electro-mechanical Systems* Vol. 34 (CRC Press, 1999).
78. Mohanty, S., Pati, S. & Kar, S. K. Improved islanded microgrid performance with sliding mode controller based electric spring. *Renew. Energy Focus* 100535 (2024).
79. Jena, N. K. et al. Fuzzy adaptive selfish herd optimization based optimal sliding mode controller for frequency stability enhancement of a microgrid. *Eng. Sci. Technol. Int. J.* **33**, 101071 (2022).
80. Pan, J.-S. et al. Gannet optimization algorithm: A new metaheuristic algorithm for solving engineering optimization problems. *Math. Comput. Simul.* **202**, 343–373 (2022).

Acknowledgements

This research is funded by European Union under the REFRESH—Research Excellence For Region Sustainability and High-Tech Industries Project via the Operational Programme Just Transition under Grant CZ.10.03.01/00/22_003/0000048; in part by the National Centre for Energy II and ExPEDite Project a Research and Innovation Action to Support the Implementation of the Climate Neutral and Smart Cities Mission Project TN02000025; and in part by ExPEDite through European Union's Horizon Mission Programme under Grant 101139527. The authors would like to express their sincere gratitude to Stanislav Misak for his exceptional supervision, project administration, and overall guidance throughout the course of this project. His expertise and support were instrumental to its success.

Author contributions

Benazeer Begum, Narendra Kumar Jena: Conceptualization, Methodology, Software, Visualization, Investigation, Writing- Original draft preparation. Binod Kumar Sahu: Data curation, Validation, Supervision, Resources, Writing—Review & Editing. Mohit Bajaj, Vojtech Blazek, Lukas Prokop: Project administration, Supervision, Resources, Writing—Review & Editing.

Declarations

Competing interests

The authors declare no competing interests.

Additional information

Supplementary Information The online version contains supplementary material available at https://doi.org/10.1038/s41598-025-89025-w.

Correspondence and requests for materials should be addressed to B.K.S. or M.B.

Reprints and permissions information is available at www.nature.com/reprints.

Publisher's note Springer Nature remains neutral with regard to jurisdictional claims in published maps and institutional affiliations.